

Image Cover Sheet

CLASSIFICATION

UNCLASSIFIED

SYSTEM NUMBER

155076

**TITLE**

COMPUTER MODELLIN GOF HEAT FLOW FOLLOWING LASER SURFACE MELTING

System Number:**Patron Number:****Requester:****Notes:****DSIS Use only:****Deliver to:**

UNLIMITED DISTRIBUTION



National Defence
Research and
Development Branch

Défense nationale
Bureau de recherche
et développement

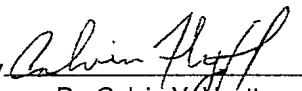
DREA CR/95/436

COMPUTER MODELLING OF HEAT FLOW FOLLOWING LASER SURFACE MELTING

by
S.B. Liu — Q. Liu — K.D. Mackay — M. W. Chernuka

MARTEC Limited
1888 Brunswick Street, Suite 400
Halifax, Nova Scotia, Canada
B3J 3J8

Scientific Authority


Dr. Calvin V. Hyatt

August 1995

W7707-4-3145/01-HAL
Contract Number

CONTRACTOR REPORT

Prepared for

**Defence
Research
Establishment
Atlantic**



**Centre de
Recherches pour la
Défense
Atlantique**

Canada

ABSTRACT

A transient three-dimensional heat transfer program called LASER1 which describes the thermal history of a specimen after laser treatment with a scanned continuous laser, has been developed following the experimentally verified method of A.F.A. Hoadley, M. Rappaz and M. Zimmerman [3]. The program was based on the conservation of energy for the treated specimen, and the three-dimensional implicit finite difference method. The surface of the melting pool was assumed to be flat. The fluid dynamics effects of the melting pool were neglected. The properties of the treated material were assumed to be linear functions of temperature for solid phase, but independent of temperature for the liquid phase. A windows-based and easy-to-user interface program, was also developed to guide the users with the provision of the temperature dependent thermal and optical properties of the material, with the provision of the laser beam and operational parameters and with the display of the computational results. The program developed in this report was used to simulate the laser surface melting for the eutectic alloy Al-Cu 33 over a range of traversing speeds between 0.2 to 5.0 m/s. Excellent agreement has been obtained from the comparison between the current simulation results, and the simulation and the experimental results obtained in Reference [3]

RÉSUMÉ

Un programme de représentation des échanges transitoires de chaleur appelé LASER1, qui décrit le comportement thermique dans le temps d'une éprouvette après un traitement au faisceau balayeur d'un laser continu, a été élaboré selon la méthode, vérifiée expérimentalement, d'A.F.A. Hoadley, de M. Rappaz et de M. Zimmerman [3]. Le programme repose sur le principe de la conservation d'énergie de l'éprouvette traitée et sur la méthode tridimensionnelle des différences finies implicites. On a présumé que la surface du bain de matériau en fusion était plane sans tenir compte des effets de dynamique des fluides. On a supposé que les propriétés du matériau traité étaient des fonctions linéaires de la température à l'état solide, mais indépendantes de la température à l'état liquide. Une interface d'utilisation conviviale en environnement Windows a aussi été élaborée pour guider l'utilisateur dans le choix des propriétés thermiques et optiques thermodépendantes du matériau, des paramètres du faisceau laser, des paramètres de fonctionnement et de la présentation des résultats des calculs. Le programme élaboré dans le présent rapport a permis de simuler la fusion par laser de la surface de l'alliage eutectique d'Al-Cu 33, pour une plage de vitesse de balayage de 0,2 à 5,0 m/s. Les résultats de la simulation corroborent ceux des simulations et des expériences cités en [3].

TABLE OF CONTENTS

ABSTRACT	ii
TABLE OF CONTENTS	iii
LIST OF TABLES	v
LIST OF FIGURES	v
 1. INTRODUCTION	 1.1
2. THE HEAT-FLOW MODEL	2.1
2.1 The Physical Model	2.1
2.2 Finite Difference Grid	2.5
3. NUMERICAL FORMULATIONS	3.1
3.1 The System of Equations for the Interior Grid Points	3.1
3.2 The System of Equations for the Grid Points on the Boundary	3.2
3.3 The Solution of the System Equations	3.4
4. INPUT DATA FOR THE PROGRAM LASER1	4.1
5. SIMULATION RESULTS AND VALIDATION FOR THE PROGRAM LASER1	5.1
6. DEVELOPMENT OF GRAPHICAL USER INTERFACE (GUI) FOR THE LASER1 PROGRAM	6.1
6.1 Development of the GUI System for LASER1 Program	6.1
6.2 Description of the GUI System of LASER1 Program	6.2
6.2.1 LASER1 GUI Window	6.2
6.2.2 Menu	6.2
6.2.3 Input Data Checking and Program Monitoring	6.4
7. A PROPOSED APPROACH FOR ANALYSIS OF HEAT FLOW RESULTING FROM LASER CLADDING WITH A WIRE FEED	7.1
7.1 The Physical Model	7.1
7.2 The Governing Equations	7.2
7.3 The Solution Methods	7.2
8. CONCLUSIONS	8.1
9. REFERENCES	9.1
APPENDIX A: THERMOCHEMICAL AND OPTICAL DATA FOR ALUMINUM BRONZES, COPPER NICKEL ALLOYS AND GUN STEELS ..	A.1
APPENDIX B: USER'S GUIDE FOR THE PROGRAM LASER1	B.1

LIST OF TABLES

TABLE 5.1: Laser-Processing Conditions for Eutectic Alloy Al-Cu33 Wt Pct	5.5
TABLE 5.2: Thermophysical Data for Eutectic Alloy Al-Cu33 Wt Pct	5.5

LIST OF FIGURES

FIGURE 2.1: A Specimen Treated by a Laser Beam Travelling with a Speed v_b . . .	2.6
FIGURE 2.2: Finite Difference Grid for the Problem as Shown in Figure 2.1	2.7
FIGURE 2.3: Phase Diagram for an Alloy	2.8
FIGURE 2.4: The Cross-Section Views of the Simulated Energy Distributions: (a) the Gaussian Distribution, (b) the Uniform Distribution	2.9
FIGURE 3.1: A Grid Point, C and its Six Neighbouring Grid Points, W,E,F,B,S and N	3.5
FIGURE 5.1: Steady-State Temperature Contours Surrounding the Melted Pool for a Traversing Velocity of 1.0 m/s	5.6
FIGURE 5.2: Dimensionless Maximum Half Width of the Melted Pool Versus Processing Time	5.7
FIGURE 5.3: Dimensionless Maximum Half Depth of the Melted Pool Versus Processing Time	5.8
FIGURE 5.4: Transverse Sectional View of the Remelted Trace for Traversing Velocities of (a) 0.5 m/s, (b) 1.0 m/s and (c) 2.0 m/s	5.9
FIGURE 5.5: Top Surface View of the Melted Pool for Traversing Velocities of (a) 0.2 m/s and (b) 0.5 m/s	5.10
FIGURE 5.6: Temperature History for the Grid Points Underneath the Melted Pool Travelling With a Speed of 0.5 m/s	5.11
FIGURE 5.7: Temperature History for the Grid Points Underneath the Melted Pool Travelling With a Speed of 1.0 m/s	5.12
FIGURE 5.8: Temperature History for the Grid Points Underneath the Melted Pool Travelling With a Speed of 2.0 m/s	5.13
FIGURE 7.1: Process Schematic Showing the Longitudinal Section of the Laser Affected Region During Laser Cladding by a Wire Feed	7.4
FIGURE B.1: Main Menu of the Program LASER1	B.5
FIGURE B.2: The Submenu Prompt Following the Selection of the Item "File" in the Main Menu	B.6
FIGURE B.3: The Submenu Prompt Following the Selection of the Item "File Prefix" in the Main Menu	B.7

LIST OF FIGURES (Continued)

FIGURE B.4: The Submenu Prompt Following the Selection
of the Item "Laser" in the Main Menu B.8

FIGURE B.5: The Submenu Prompt Following the Selection
of the Item "Material" in the Main Menu B.9

FIGURE B.6: The Submenu Prompt Following the Selection
of the Item "New Material" in the Main Menu B.10

FIGURE B.7: The Submenu Prompt Following the Selection
of the Item "Grid" in the Main Menu B.11

FIGURE B.8: The Submenu Prompt Following the Selection
of the Item "New Mesh" in the Main Menu B.12

FIGURE B.9: The Dialogue Box Prompt Following the Selection
of the Item "Analysis" in the Main Menu B.13

FIGURE B.10: The Submenu to Confirm the Start of the Analysis B.14

FIGURE B.11: The Main Menu Following Analysis Completion B.15

FIGURE B.12: The Submenu Prompt Following the Selection
of the Item "Graphics" in the Main Menu B.16

FIGURE B.13: Grid and Laser Power Distributions B.17

FIGURE B.14: 3-D Temperature Contours B.18

FIGURE B.15: Temperature Contours on the Top Surface B.19

FIGURE B.16: Temperature Contours on the Centre Plane B.20

FIGURE B.17: Plan View of the Melt-Pool B.21

FIGURE B.18: Transverse View of the Melt-Pool B.22

FIGURE B.19a: A Point Selected on the Transverse Section
Through the Weld-Pool B.23

FIGURE B.19b: Temperature Time History for User Selected Point B.24

1. INTRODUCTION

Laser surface melting has many promising applications [1-2] because of its ability to alter, with accuracy, the properties of very localized surface regions without reprocessing the whole material. The fine grain sizes and reduction of segregation, the solid solution extension, and the metastable phases which result from this technology, improve the surface sensitive properties of a material, such as erosion, corrosion, and wear resistance. However, the scale of such operations makes in-situ measurements of the process variables difficult. Most information about laser surface modification is thus obtained by studying the after effects, such as the change to the microstructure and the mechanical or chemical properties of the treated surface. Therefore, modelling the physical process, and, particularly, the thermal history of the specimen treated by a moving high-power laser beam, can help better understand some of the effects produced by laser treatment. Furthermore, modelling work can reduce substantially the time required for process control and optimization.

In general, the heat flow resulting from laser surface melting is a transient three-dimensional heat transfer problem, also, involving latent heat. For the past decade or so, many investigations [3-12] have been made to simulate this type of heat flow in either the laser surface melting process or in the laser welding process. Among the most commonly cited ones, Kou and Wang [6] carried out a computer simulation to describe three-dimensional melted pools for the case where the workpiece is moving with respect to the laser beam. Their mathematical model assumed that the melted pool was stationary in space but travelled with respect to the specimen. The finite difference method based on the equations of mass, momentum, energy, and the heat transfer boundary conditions was used to obtain the size of melted pools. The driving forces of the buoyancy force and the surface tension gradient at the pool surface for flow were also considered in their model. They achieved good agreement between the simulation and the observations, for a melted pool for a 6063 aluminum sheet travelling at a single speed of 4.23 mm/s. Paul and Debroy [7] presented a two-dimensional simulation of the temperature profiles and fluid flow fields in a weld pool for low power

1.2

continuous laser welding, through the finite difference solution of the Navier-Stokes equation and the equation of conservation of energy. Their model predictions were compared with experimentally determined melt pool shape, surface profile and microstructure. The agreement with the experimental remelted profile was not particularly good, probably due to their two-dimensional simulation. On the other hand, the predicted dendrite arm spacing was close to that observed. The computational model of Paul and Debroy [7] was later modified by Zacharia et al. [8] to investigate the heat transfer conditions during Nd:Yag pulsed laser welding of austenitic stainless steels. Their two-dimensional simulation also gave good agreement for the microstructure, but with only qualitative agreement for the melt pool shape.

Recently, Hoadley, Rappaz and Zimmermann [3] presented a transient three-dimensional conduction-based heat-flow model to simulate the heat flow during laser surface melting for the eutectic alloy Al-Cu 33 Wt Pct over a range of traversing speeds between 0.2 and 5.0 m/s. The finite difference method based on the conservation of energy and the heat transfer boundary conditions, was used to compute the detailed melted pools and the temperature fields. Excellent agreement with the experimental data was found over the range of processing speeds for the maximum melt pool dimensions, the transverse profile of the laser trace, the melt surface shape, and the resolidified microstructural spacings. Compared with the other models, the model given by Hoadley, Rappaz and Zimmermann [3] seems to be very reliable, and yet does not require excessive computational effort.

Martec Limited was contracted by DREA to develop a computer program, following the methods given by Hoadley, Rappaz and Zimmermann [3], to describe the thermal history of the specimen after laser treatment with a scanned continuous laser. Consequently, Martec personnel developed the computer program suite LASER1 to meet this objective. In this report, the formulations used in the program LASER1 are presented in detail. The laser surface melting for the eutectic alloy, Al-Cu 33 Wt Pct, under the experimental processing conditions as specified in Reference [3], was simulated by using the program LASER1 to

validate the program. Provided under separate cover is the source code of the program LASER1.

As required, the temperature dependent data for a common low alloy steel, a common stainless steel, an aluminum alloy 2024, an Al-Cu 33 Wt Pct alloy, a series of copper-nickel alloys containing 1, 3, 5, 10, 20 and 30 weight % nickel and nickel aluminum bronze are also included in the program LASER1, and in Appendix A of this report.

2. THE HEAT-FLOW MODEL

2.1 The Physical Model

Figure 2.1 shows schematically the modelled region Ω , and the laser beam travelling with a velocity of v_b . The physical model considers only the heat-affected zone around the laser beam and implicitly assumes that the workpiece is significantly larger than this volume. An Eulerian coordinate system (x,y,z) was attached to the laser beam. In such a coordinate system, the workpiece is assumed to be moving along the x -axis with a velocity $-v_b$, the z -axis is coincident with the central line of the laser beam, and the plane $z=0$ is the top-surface of the workpiece. Since the problem is symmetrical with respect to the plane $y=0$, only half of the workpiece ($y > 0$) needs to be modelled. The equation of energy for the material moving with velocity, $-v_b$, relative to the laser beam is given by

$$\frac{\partial H}{\partial t} - v_b \frac{\partial H}{\partial x} = \text{div}(k(T) \text{ grad}(T)) \quad (2.1)$$

where k is the temperature-dependent conductivity. Note that any convection due to fluid flow in the molten region is not considered here. Fluid dynamics in the melted pool is also ignored.

Average or enthalpy methods offer a versatile approach for modelling phase change problems. By assuming that phase equilibrium exists everywhere, conditions within the processed material are given directly by the temperature or enthalpy of the material, thus avoiding any necessity to locate phase boundaries. The relationship between temperature, T , and enthalpy, H , is given by

$$H(T) = \int_0^T c(T) dT + (1 - f_s(T))L \quad (2.2)$$

where $c(T)$ and L are the volumetric specific heat and latent heat, respectively. The solid fraction f_s is assumed to be a step function in the case of eutectic solidification, as occurs with

2.2

pure or eutectic material. In the case of dendritic solidification, f_s may be deduced from a Scheil equation [26].

$$wC_O (1 - f_s)^{w-1} = C_S \quad (2.3)$$

where C_O is the alloy composition at the ambient temperature, C_S is the alloy composition at a temperature T , between the solidus temperature T_S and the liquidus temperature T_L , and w is the equilibrium partition ratio of C_S to the alloy composition for the liquidus phase C_L , i.e.,

$$w = C_S/C_L \quad (2.4)$$

When the liquidus and solidus are straight lines emanating from the composition of the pure solvent ($C_O=0$) as in Figure 2.3, w is constant. Furthermore, if w is less than unity, that is, the phase diagram is as shown in Figure 2.3 with solidus and liquidus sloping downward to the right, w can be obtained from the phase diagram for the alloy, and from the same phase diagram, C_S is derived as follows:

$$C_S = C_O \frac{T_L - (1 - w)T - wT_S}{T_L - T_S} \quad (2.5)$$

Substituting Equation (2.5) into Equation (2.3), the following equation is obtained for f_s :

$$(1 - f_s)^{w-1} = \frac{T_L - (1 - w)T - wT_S}{w(T_L - T_S)} \quad (2.6)$$

Note that Equation (2.6) is applicable only when $w < 1$. For the sake of versatility and simplicity, in the program LASER1, f_s is obtained from the following equation of interpolation:

$$(f_s) = \frac{T_L - T}{(T_L - T_S)} \quad (2.7)$$

When the difference between T_L and T_S is relatively small, as for copper nickel alloys, the volume composition of the dendritic phase within Ω is much smaller than either the volume of solidus phase or the volume of liquidus phase, the approximation made for f_s should not

result in a significant error. Equation (2.7) is used only when T is between T_S and T_L . Obviously, $f_s=1$ when T is below T_S and $f_s=0$ when T is higher than T_L .

Equations (2.1) and (2.2) are solved within the region Ω with the internal boundaries Γ_1 chosen so that the temperature at the boundary of the calculation domain is close to the initial temperature T_a of the base material. More precisely, at any time, the boundary condition at Γ_1 is specified by the Rosenthal point source model [21]:

$$T(x,r) = T_a + \frac{\bar{\beta}P}{2\pi\bar{k}r} \exp\left\{\frac{-v_b(x+r)}{2\bar{\alpha}}\right\} \quad (2.8)$$

where r is the radial distance from the point heat source, P is the power of the heat source, and $\bar{\alpha}$, $\bar{\beta}$, and \bar{k} are the average thermal diffusivity, surface absorption, and thermal conductivity, respectively. Equation (2.8) is used in the program LASER1 to specify the temperature on the boundary Γ_1 , where r is measured from the origin of the Eulerian coordinate system and P is taken to be the power of the laser beam.

The surface of the material Γ_2 is assumed to remain flat during laser remelting. Thus the effects of surface tension and gas pressure on the liquid region can be neglected. The laser energy is distributed over a small circular region on Γ_2 , the size of which depends on the configuration of the specific laser and the optical characteristics of its focusing mirrors. To accurately simulate the condition of the heat source distribution in the immediate vicinity of the beam, the model utilizes a normalized one-dimensional radial function $F(\rho)$, i.e.

$$2\pi \int_0^\infty F(\rho) \cdot \rho d\rho = 1 \quad (2.9)$$

$F(\rho)$ may be given by a polynomial or summation of Gaussian functions which best fit the particular laser energy distribution. This function is then numerically integrated in order to find the local energy, q_i , impinging on each finite difference grid, say, i :

$$q_i = P \int_{\Delta X_i} dx \int_{\Delta Y_i} dy \cdot F(\rho(x,y)) \quad (2.10)$$

2.4

where ΔX_i and ΔY_i are length and width (i.e., along the x- and y-axes), respectively, of the i-th finite difference grid.

For the program LASER1, the function $F(\rho)$ represents the summation of three Gaussian distributions. One distribution is centred on the axis $x = 0$ and the other two are offset an equal distance to either side. The superposition of the three curves is rotated about the axis $x = 0$ to yield a circular distribution. In order to exactly match the energy distribution observed experimentally in Reference [3], two parameters are adjusted: the standard deviation σ of the Gaussian functions and the offset μ between the centres of each curve. Assume that a is the focal radius of the laser beam. In the program LASER1, an offset $\mu = 7/13 a$ from the origin, and a standard deviation of $2\sigma = 6/13 a$ are used, and the function $F(\rho)$ is finally defined as

$$F(\rho) = \frac{A}{\sqrt{2\pi}\sigma} \{ \exp(-\rho^2/2\sigma^2) + \exp(-(\rho + \mu)^2/2\sigma^2) + \exp(-(\rho - \mu)^2/2\sigma^2) \} \quad (2.11)$$

where A is determined by substituting Equation (2.11) into Equation (2.9) and solving. An alternate choice of the function $F(\rho)$ in the program LASER1, is a normalized step function over the laser-beam-focalized circular area with a radius a . The cross-section views of the simulated energy distributions, by the two different functions $F(\rho)$, are shown in Figure 2.4.

Since there is also heat loss to the surroundings by natural convection and radiation, the boundary condition on the surface Γ_2 is given by

$$k \frac{\partial T}{\partial z} = \beta(T) P F(\rho) - h(T) (T(x,y) - T_a) \quad (2.12)$$

where $h(T)$ is a temperature-dependent heat-transfer coefficient and $\beta(T)$ is the temperature-dependent surface absorption. It is noted from Equation (2.12) that the heat loss by radiation and fluid flow is neglected.

As only half of the laser trace is modelled, an adiabatic boundary condition is set on the longitudinal plane of symmetry Γ_3 . The initial temperature of the material is simply assumed to be the ambient temperature T_a .

2.2 Finite Difference Grid

The energy equation, Equation (2.1), is solved using a finite difference scheme on an orthogonal grid in three dimensions. This orthogonal grid as shown in Figure 2.2, is automatically generated by the program LASER1. The dimensions of the grid in x direction, y direction and z direction, are chosen to be approximately 18, 4 and 3 times of the laser focal radius, respectively. A refinement of the grid is made near the region heated by the laser beam, and the region behind the laser beam ($x < 0$) because the higher temperatures are expected in these regions according to Reference [3].

2.6

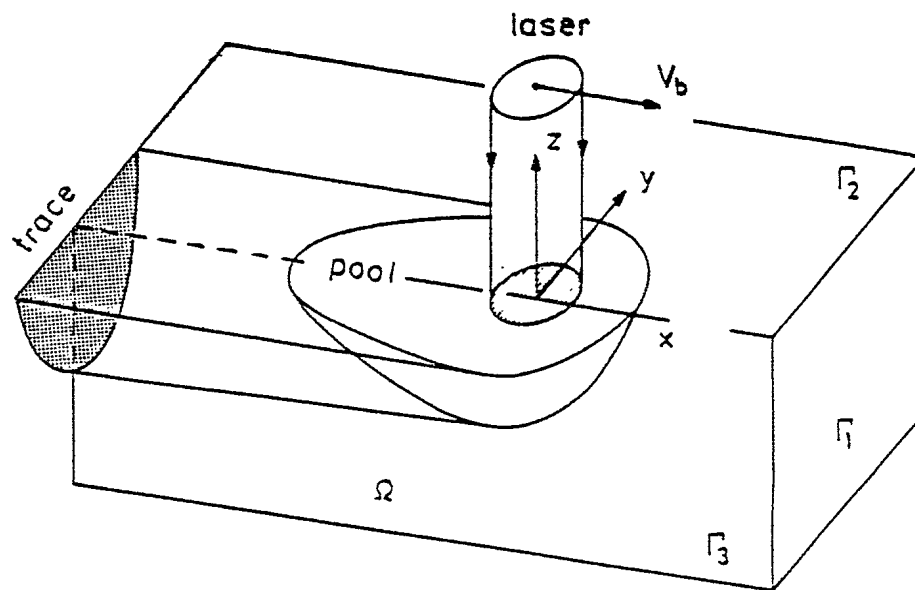


FIGURE 2.1: A Specimen Treated by a Laser Beam Travelling with a Speed v_b

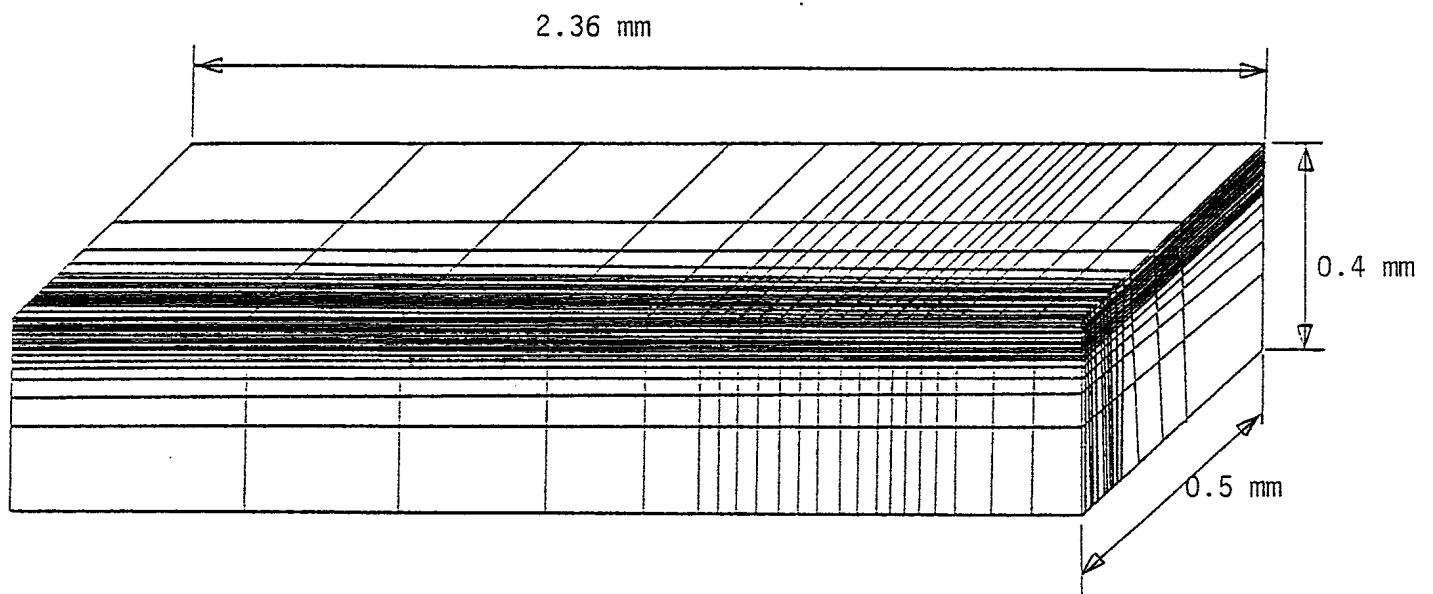


FIGURE 2.2: Finite Difference Grid for the Problem as Shown in Figure 2.1

2.8

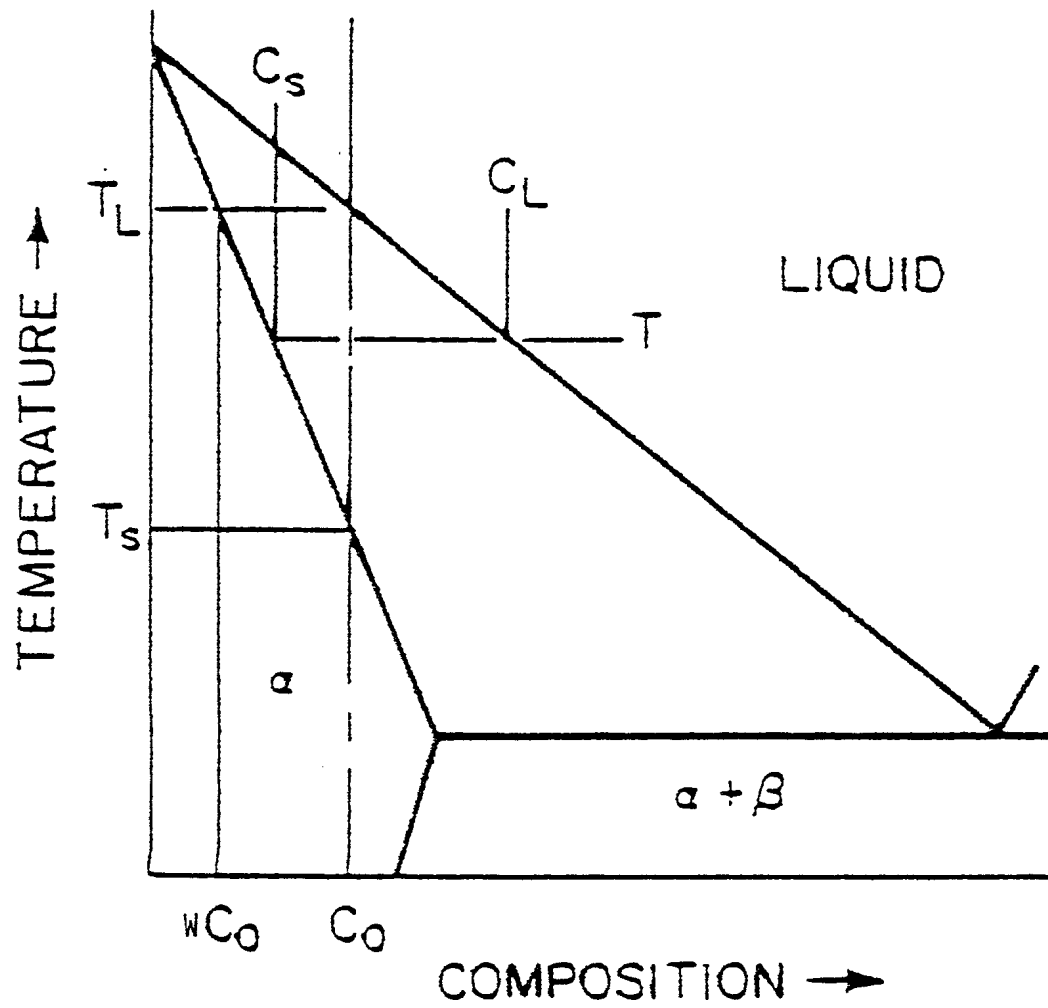
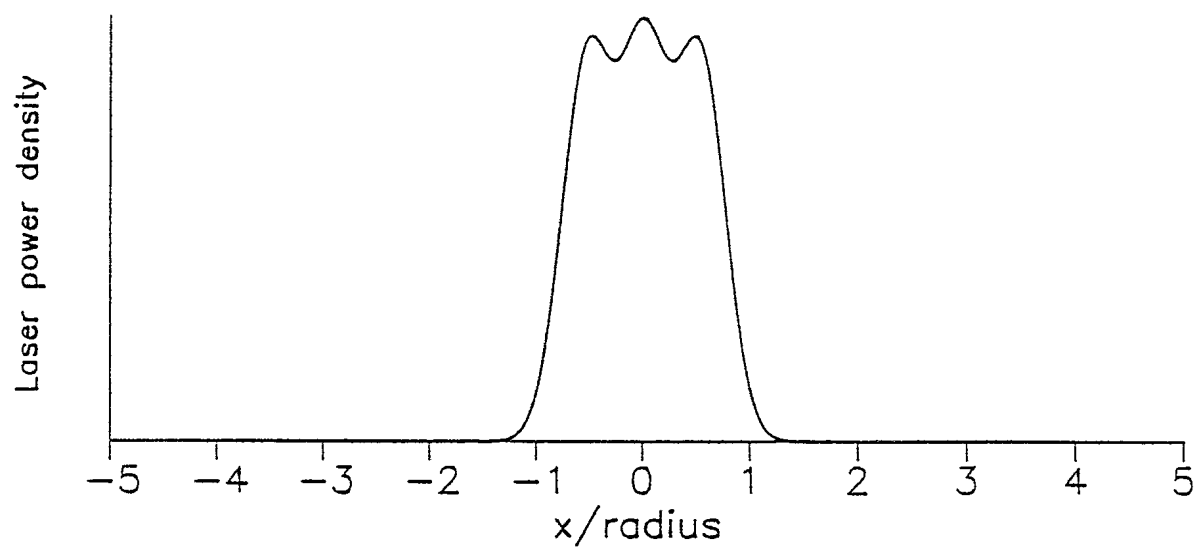
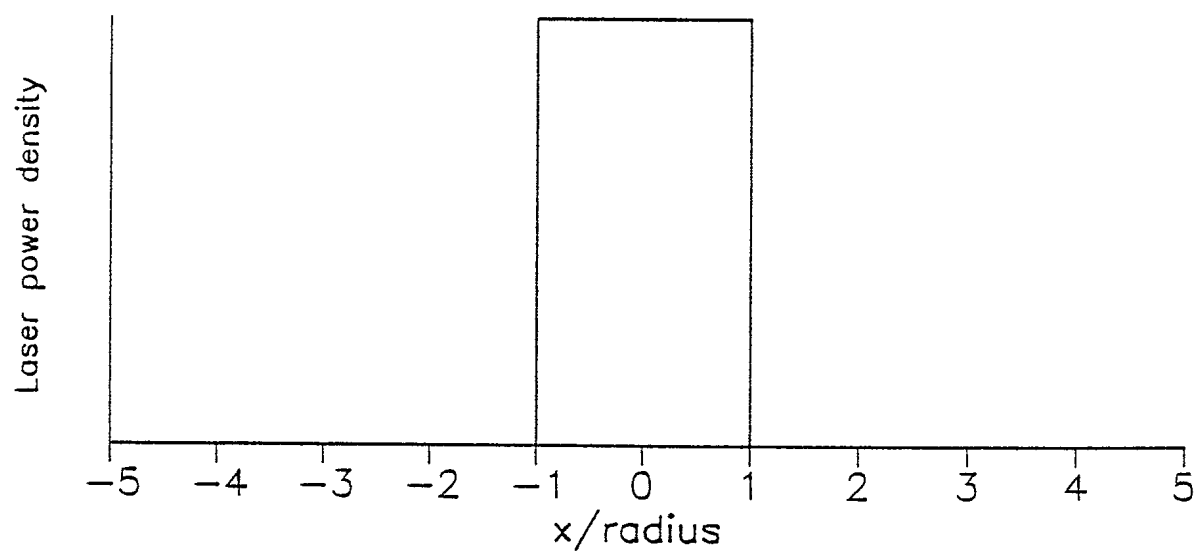


FIGURE 2.3: Phase Diagram for an Alloy



(a)



(b)

FIGURE 2.4: The Cross-Section Views of the Simulated Energy Distributions:
(a) the Gaussian Distribution, (b) the Uniform Distribution



3. NUMERICAL FORMULATIONS

3.1 The System of Equations for the Interior Grid Points

Considering a grid point, C, within the region Ω , and its six neighbouring grid points, W, E, F, B, S and N as shown in Figure 3.1, Equation (2.1) can be integrated over the volume, $\Delta X \Delta Y \Delta Z$, of this grid point. The sides of volume are defined as follows:

$$\begin{aligned}\Delta X &= \frac{1}{2}(\Delta X_W + \Delta X_E) \\ \Delta Y &= \frac{1}{2}(\Delta Y_F + \Delta Y_B) \\ \Delta Z &= \frac{1}{2}(\Delta Z_S + \Delta Z_N)\end{aligned}\tag{3.1}$$

where ΔX_W and ΔX_E are the distances between the grid points C and W and between C and E, respectively. The grid points C, W and E have the same Y and Z coordinates, but have different X coordinates. ΔY_F , ΔY_B , ΔZ_S and ΔZ_N are similarly defined.

Applying the divergence theorem and integrating $(\partial H / \partial x) \cdot dx$, the following relationship is obtained:

$$\Delta X \Delta Y \Delta Z \frac{\partial H}{\partial t} = \int_{\Gamma_c} k(T) \cdot \text{grad } T \cdot \mathbf{n} \cdot dT_c + v_b \cdot \int_{\Delta Y} dy \int_{\Delta Z} dz \cdot [H_R - H_L] \tag{3.2}$$

where \mathbf{n} is the unit vector normal to the volume surface, Γ_c , and H_R and H_L represent the average enthalpy to the right and left of C, respectively. Introducing an upwind parameter, θ , see, eg. Thomasset [20], the enthalpy difference in Equation (3.2) can be written as

$$v_b \cdot \int_{\Delta Y} dy \int_{\Delta Z} dz \cdot [H_R - H_L] = v_b \cdot \Delta Y \Delta Z \cdot [H_E \theta + H_c(1 - 2\theta) + H_w(\theta - 1)] \tag{3.3}$$

where $1/2 \leq \theta \leq 1$. Taking the fully implicit backward difference time discretization, see, eg. Meyers [23], and using Equation (3.3), Equation (3.2) becomes

3.2

$$\begin{aligned}
& k_{EC} \frac{\Delta Y \Delta Z}{\Delta X_E} (T_E^{n+1} - T_C^{n+1}) + k_{WC} \frac{\Delta Y \Delta Z}{\Delta X_W} (T_W^{n+1} - T_C^{n+1}) + k_{NC} \frac{\Delta X \Delta Y}{\Delta Z_N} (T_N^{n+1} - T_C^{n+1}) \\
& + k_{SC} \frac{\Delta X \Delta Y}{\Delta Z_S} (T_S^{n+1} - T_C^{n+1}) + k_{FC} \frac{\Delta X \Delta Z}{\Delta Y_F} (T_F^{n+1} - T_C^{n+1}) + k_{BC} \frac{\Delta X \Delta Z}{\Delta Y_B} (T_B^{n+1} - T_C^{n+1}) \quad (3.4) \\
& + V_B \cdot \Delta Y \Delta Z \cdot [H_E^{n+1} \theta + H_C^{n+1} (1 - 2\theta) + H_W^{n+1} (\theta - 1)] = \Delta X \Delta Y \Delta Z \frac{H_C^{n+1} - H_C^n}{\Delta t}
\end{aligned}$$

where n represents the time-step and Δt is the time increment. The thermal conductivities appearing in Equation (3.4), k_{iC} with $i = E, W, N, S, B, F$, corresponds to $k(T_{iC})$ taken at the midtemperature, $T_{iC} = (T_i + T_C)/2$. Following Thomasset [20], a stable and accurate scheme can be obtained for the linear case, i.e., when $H(T) = cT$ with

$$\theta = \frac{1}{2} \left[1 + \text{Coth} \left(\frac{\gamma}{2} \right) \right] - \frac{1}{\gamma} \quad \text{with} \quad \gamma = \frac{v_b \cdot \Delta X}{k/c} \quad (3.5)$$

A Newton method is employed to linearize the enthalpy as a function of the temperature in Equation (3.4), so that

$$H^{n+1} = H^n + c(T^n) \cdot (T^{n+1} - T^n) \quad (3.6)$$

Substituting Equation (3.6) into Equation (3.4), a system of linear equations containing the unknown temperatures for all the interior grid points at the time step $(n+1)$ can be obtained. Once the temperatures are known, the enthalpies can be obtained by using Equation (2.2).

3.2 The System of Equations for the Grid Points on the Boundary

Accounting for the boundary conditions for a grid point, say, C on Γ_1 , the temperature T at this grid point is obtained from Equation (2.7). In the program LASER1, the following equation is used to specify the known temperature:

$$K \cdot T^{n+1} = K \cdot T_o \quad (3.7)$$

where K is a very large number, 10^{20} , and T_0 is the value of the temperature computed from Equation (2.7). Thus, a system of equations such as Equation (3.7) can be obtained for all the grid points on Γ_1 .

Accounting for the energy balance for a grid point, C , on Γ_2 , and also taking the backward difference approximation leads to the following equations:

$$q = q_W + q_E + q_F + q_B + q_N + c \Delta X \Delta Y \Delta Z \frac{T_c^{n+1} - T_c^n}{\Delta t} \quad (3.8)$$

where

$$\begin{aligned} q &= [\beta PF - h \cdot (T_C^{n+1} - T_a)] \Delta X \Delta Y \\ q_W &= \Delta Y \Delta Z \cdot k_{WC} \cdot (T_C^{n+1} - T_W^{n+1}) / \Delta X_W \\ q_E &= \Delta Y \Delta Z \cdot k_{EC} \cdot (T_C^{n+1} - T_E^{n+1}) / \Delta X_E \\ q_F &= \Delta X \Delta Z \cdot k_{FC} \cdot (T_C^{n+1} - T_F^{n+1}) / \Delta Y_F \\ q_B &= \Delta X \Delta Y \cdot k_{BC} \cdot (T_C^{n+1} - T_B^{n+1}) / \Delta Z_N \end{aligned}$$

Note that $q_F = 0$ if the grid point C is at the intersection of the boundary Γ_2 and the boundary Γ_3 .

Similarly, for the boundary conditions for a grid point C , on Γ_3 , accounting for the energy balance and also taking the backward difference approximation leads to the following equations:

$$q_W + q_E + q_S + q_N + q_F + c \frac{T_C^{n+1} - T_C^n}{\Delta t} \Delta X \Delta Y \Delta Z = 0 \quad (3.9)$$

where

$$q_S = \Delta X \Delta Y \cdot k_{SC} \cdot (T_C^{n+1} - T_S^{n+1}) / \Delta Z_S$$

3.4

3.3 The Solution of the System Equations

Combining Equations (3.4)-(3.9) and putting the known vectors and their products on the right-hand side, gives a system of equations which can be written as:

$$[A]\{T\}^{n+1} = \{B\}^{n+1} \quad (3.10)$$

where $[A]$ is the coefficient matrix, $\{T\}^{n+1}$ is the vector of unknown temperatures and $\{B\}^{n+1}$ is the vector of knowns resulting from the known boundary conditions and the temperature solution from the previous time step.

Equation (3.10) represents a linear banded system of equations, which can be solved by a special-purpose Gaussian elimination method, see eg. Hager [24]. The solution starts from time $t=0$, and proceeds with the next time increment Δt . The steady-state temperature field is assumed to be reached when the total change in energy within the mesh is less than 0.1% of the energy absorbed.

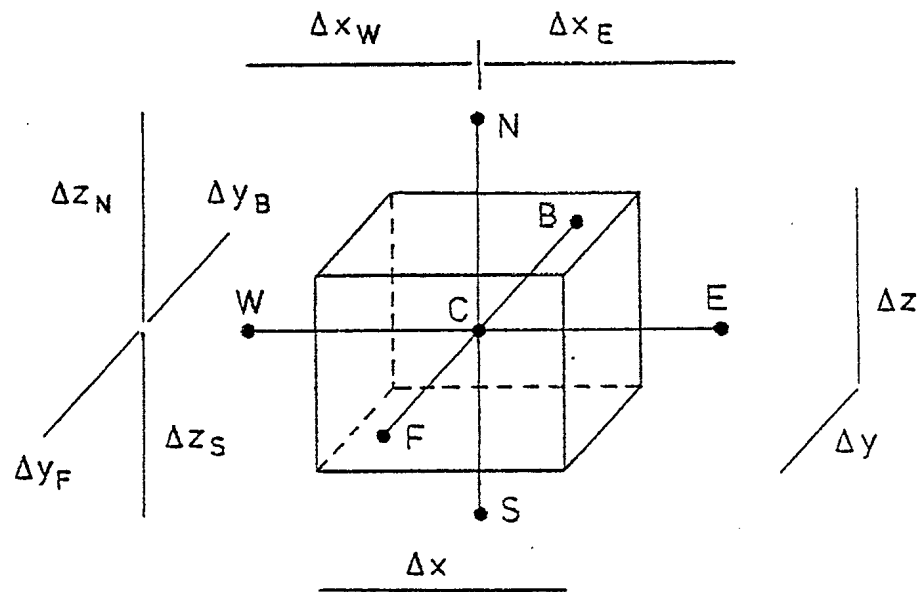


FIGURE 3.1: A Grid Point, C and its Six Neighbouring Grid Points, W, E, F, B, S and N

4. INPUT DATA FOR THE PROGRAM LASER1

The input data for this program are expected to primarily consist of the laser-processing conditions and the temperature dependent thermophysical data of the treated material. Parameters defining the laser-processing conditions include the laser power, the focal diameter, the traversing velocity, the ambient temperature, and the surface heat-transfer coefficient. The temperature dependent material data include the surface absorption for solid state and liquid state, the volumetric specific heat for solid and liquid state, and the thermal conductivities for solid state and liquid state. In addition, the input data include the equilibrium partition ratio of alloy composition of the solidus phase to the liquidus phase, the solidus temperature and liquidus temperature.

In the program LASER1, the temperature dependent data for the solid phase are assumed to be linear functions of the temperature, while they are independent of temperature (constant) for the liquid phase.



5. SIMULATION RESULTS AND VALIDATION FOR THE PROGRAM LASER1

The laser surface remelting for the eutectic alloy Al-Cu 33 Wt Pct, over a range of traversing speeds from 0.2 m/s to 5.0 m/s, was simulated by using the program LASER1. The same problem has been analyzed numerically and experimentally by Hoadley, Rappaz and Zimmermann [3]. To use their results for the comparison, the laser-processing conditions and the thermophysical data used in Reference [3], were also adopted for the current simulation. Table 5.1 lists the laser-processing conditions. The thermophysical data of alloy Al-Cu 33 Wt. Pct, are shown in Table 5.2. Note that the thermal conductivity for the liquid phase of the material was not given in Reference [3], but was obtained from Reference [25]. The finite difference grid shown in Figure 2.2 was used for the simulation.

Figure 5.1 shows an enlarged view of the steady-state temperature profile, on the top surface and the central longitudinal plane, for a traversing velocity of 1.0 m/s. Also shown in Figure 5.1 are the corresponding simulation results of Reference [3]. It can be seen from Figure 5.1 that there is a fairly good agreement between the present simulation and the simulation of Reference [3]. The maximum width of the melted pool, y_{\max} , was determined by taking the maximum perpendicular distance from the surface centreline to the first temperature contour in Figure 5.1(a). In the same way, the maximum depth of the melted pool, z_{\max} , was obtained by taking the maximum vertical distance in the longitudinal plane in Figure 5.1(b). Note, however, that the location of the point of the maximum depth is behind the point of maximum width (negative x coordinate) due to the time required for the heat to be transported from the surface to the bottom of the pool. Such a prediction is also consistent with Reference [3].

When commenting on the dimensions of the melted pools, over the whole range of processing speeds, it is convenient to use the non-dimensionalization suggested by Kou et al. [5]. Thus, the characteristic length scale is based on the beam radius, a . The nondimensional melted pool width and depth become

5.2

$$y^* = y_{\max}/a \quad (5.1)$$

$$z^* = z_{\max}/a \quad (5.2)$$

The time scale is given by the ratio of the average diffusivity to advective transport:

$$t^* = \alpha/av_b \quad (5.3)$$

The dimensionless maximum half width and depth of calculated using Equations (5.1) and (5.2), at several traversing velocities, are shown in Figure 5.2 and Figure 5.3, respectively. On these figures, data points are also shown for the experimental measurements, where the vertical error bars indicate the experimental deviation, and the calculations of Reference [3].

It can be seen in Figure 5.2 that for the maximum melt pool half widths, the agreement between the present simulation and the simulations of Reference [3] and the experiments of Reference [3], is excellent over the whole range of processing times except when $v_b = 2.0$ m/s. The maximum depths plotted in Figure 5.3 also give excellent agreement between the present simulations and the simulations of Reference [3]. For the comparison with the experimental results of Reference [3], it can also be seen from Figure 5.3 that there is a fairly good agreement for processing traversing velocities up to the minimum, i.e., 0.2 m/s. However, the trend is for the melt depths to be overpredicted by the simulation as the processing time increases. As explained in Reference [3], this may be due to an outward flow generated by capillary forces which maintains the surface of the melt at a relatively uniform temperature. By contrast in the simulation, the convection is ignored and the peak temperature on the surface increases sharply with increasing time under the laser beam. Hence, the component of the diffusive flux acting downward from the surface would be increased by comparison with a convecting melt. This would account for the greater pool depths found in the simulation. Following the same reasoning, one would expect surface convection to produce greater melting near the surface and hence increased widths of melt

pools. However, there is no apparent divergence between the experimental and the predicted maximum widths in Figure 5.2.

As explained in Reference [3], accurate predictions of the transverse section of the laser trace is important, as this outlines the exact region reprocessed by each pass of the laser. Such information is necessary when considering overlapping traces used to cover the whole of a surface region. The experimental transverse profiles in Reference [3] were digitized from transverse micrographs, and were then smoothed with a least-squares polynomial. The points are shown in Figures 5.4(a) through (c) for traversing velocities of 0.5, 1.0, and 2.0 m/s, respectively. Also shown are the points representing the interface position calculated from the numerical simulations in Reference [3] and the present investigations. For all three traversing velocities, the overall shape is reproduced well by the present simulation.

Figures 5.5(a) and (b) show the digitized curves (shown as the dashed lines) of typical surface ripples at 0.2 and 0.5 m/s taken from surface photographs in Reference [3]. The curve is taken from the top surface of the melted pool, and the points of the curve are taken to be the turning points where solidification or melting occurs. For the simulated melted surface, it is also possible to show the shape of the region near the front of the pool undergoing melting. The simulation curves from Reference [3] and the present simulation, shown as the two continuous lines with different thickness, are superimposed in Figures 5.5(a) and (b) for comparison. In both cases, the predicted surface shapes agrees well each other, and with the shape outlined by the ripples in the experiments.

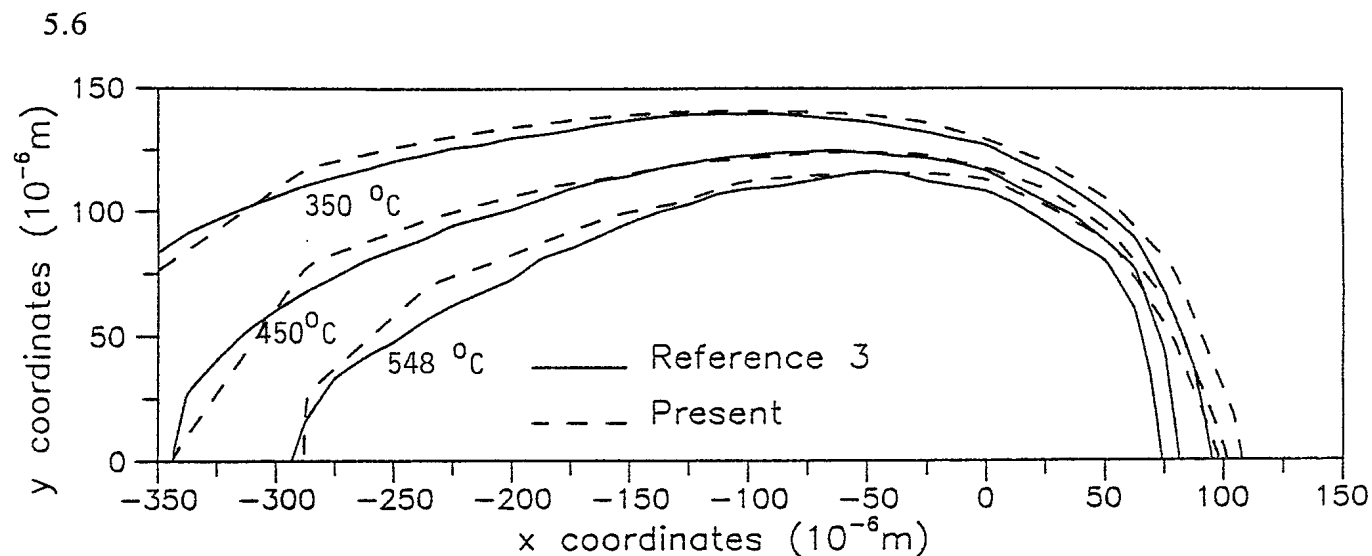
Once the steady-state temperature field is known, it is possible to compute the temperature history for the material of the specimen. Figures 5.6 to 5.8 show the temperature as a function of time for the grid points underneath the melted pools, for traversing speeds of 0.5, 1.0 and 2.0 m/s, respectively. In these figures, the temperature for a point at time equal to zero, is the temperature for the point with the same z coordinate and with $y=0$, $x=x_{\max}$ (right end), in the finite difference grid shown in Figure 2.2. The temperature for a point at

5.4

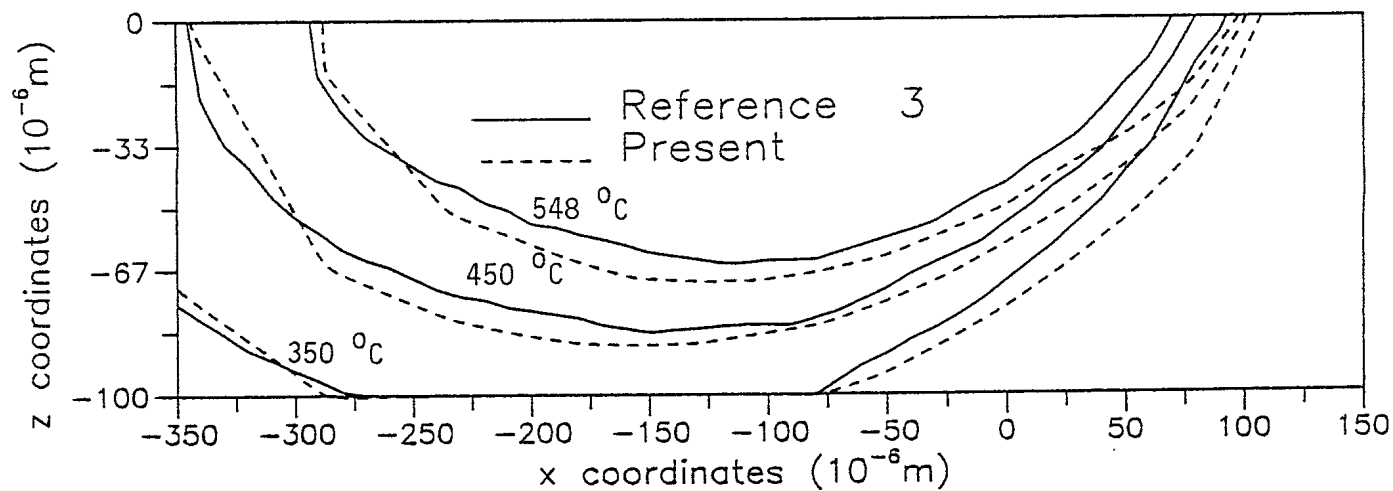
time equal to the maximum time in the figures, is the temperature for the point with the same z coordinate and with $y=0$, $x=x_{\min}$ (left end), in the finite difference grid. The temperature for a point at the other time points was thus similarly determined. As expected, for a low traversing speed, the material takes a longer time to pass through the laser beam and thus higher temperatures are obtained.

TABLE 5.1: Laser-Processing Conditions for Eutectic Alloy Al-Cu33 Wt Pct	
Laser power	1250w
Focal diameter	260 μm
Beam mode	TEM00 + TEM10*
Traverse velocity	0.2 to 5.0 m/s
Ambient temperature	20°C
Surface heat-transfer coefficient	100 W/m ² /°C
Protective gas	He

TABLE 5.2: Thermophysical Data for Eutectic Alloy Al-Cu33 Wt Pct	
Eutectic composition	32.7 Wt Pct Cu
Eutectic temperature	548.0°C
Surface absorption (solid)	$3.0 + 2.5 \times 10^{-3}T$ Pct
Surface absorption (liquid)	8.5 Pct
Density	3600 Kg/m ³
Specific heat (solid)	$2.6 \times 10^6 + 1.22 \times 10^3 T$ J/m ³ /°C
Specific heat (liquid)	2.86×10^6 J/m ³ /°C
Latent heat	1.23×10^9 J/m ³
Thermal conductivity (solid)	58.1 W/m/°C
Thermal diffusivity (average)	4.21×10^{-5} m ² /s



(a) On the Top Surface of the Specimen



(b) On the Central Longitudinal Plane

FIGURE 5.1: Steady-State Temperature Contours Surrounding the Melted Pool
for a Traversing Velocity of 1.0 m/s

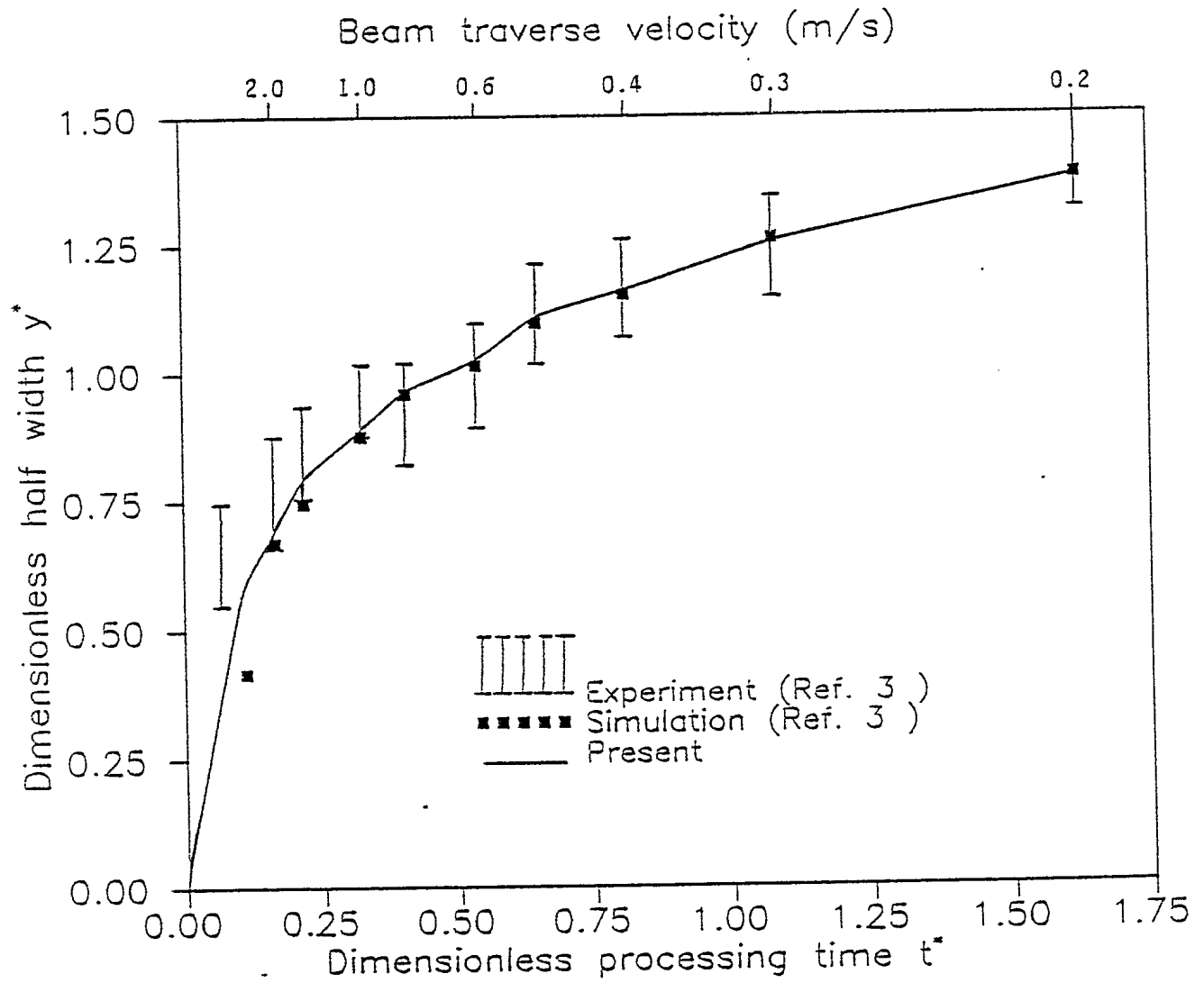


FIGURE 5.2: Dimensionless Maximum Half Width of the Melted Pool Versus Processing Time

5.8

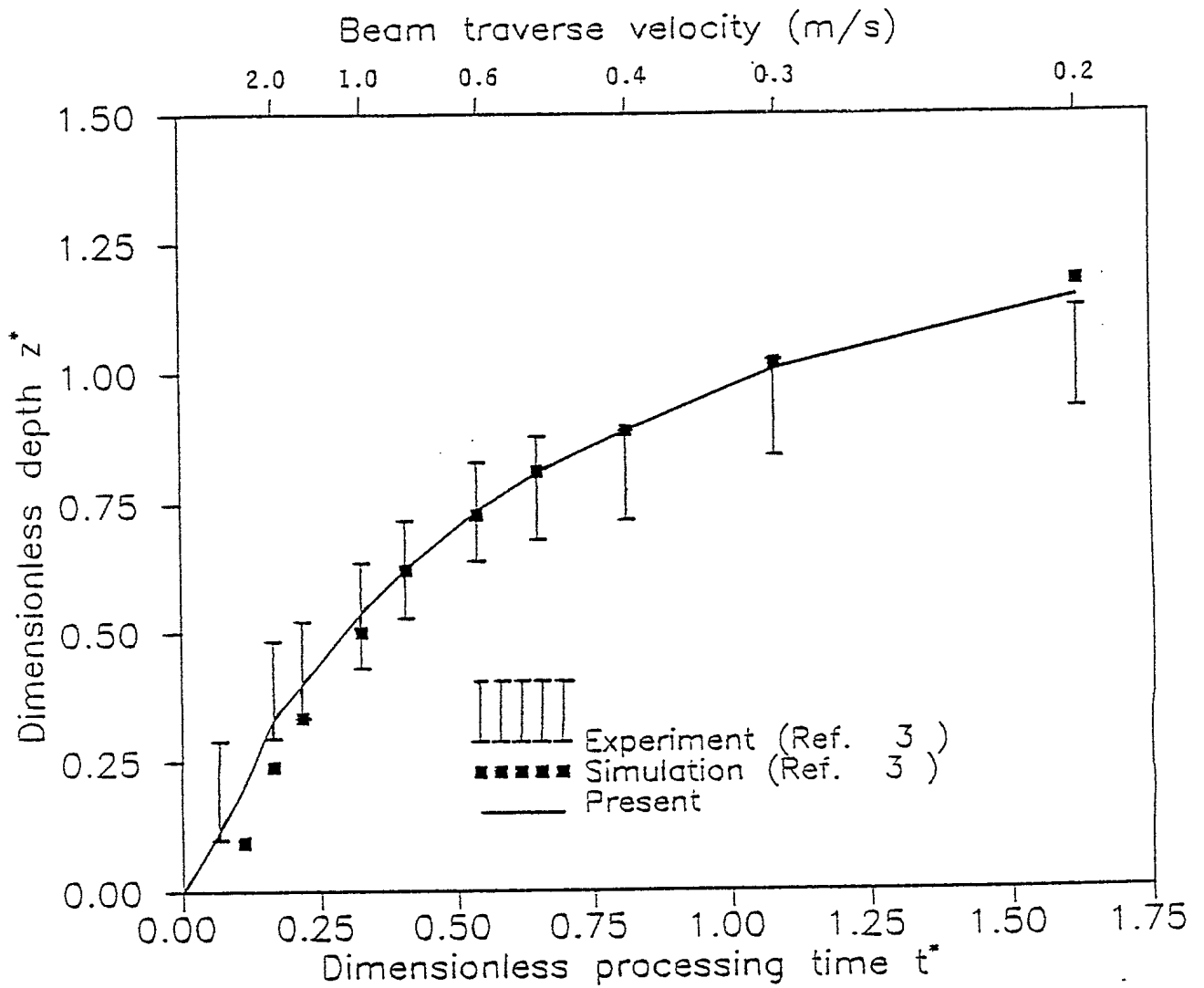
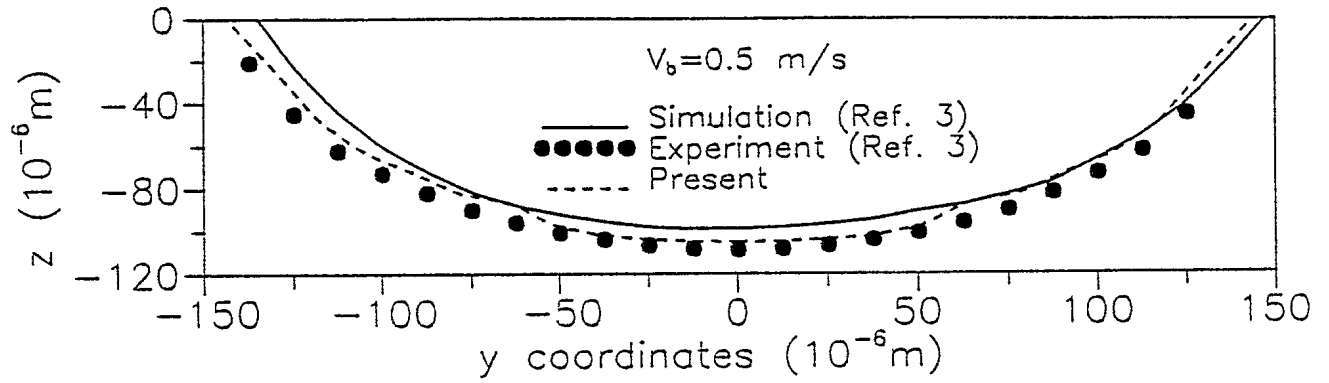
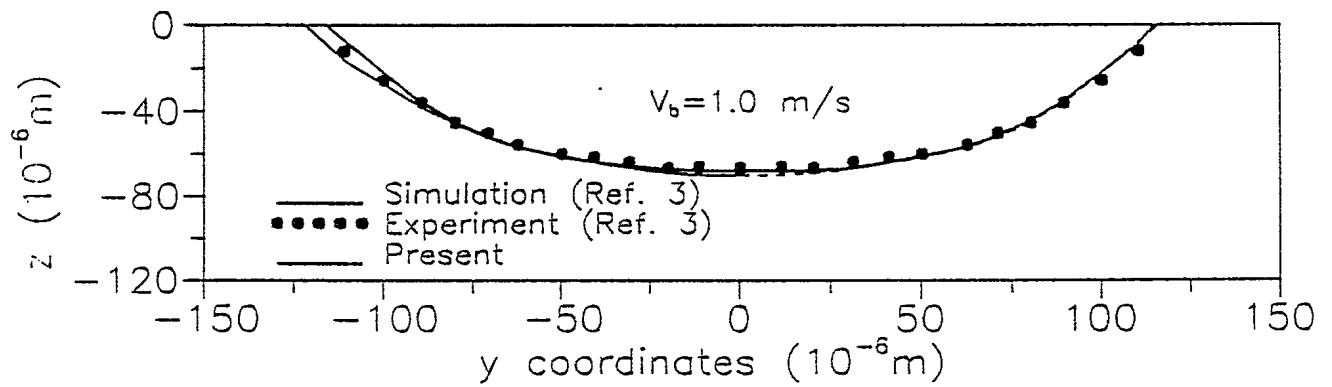


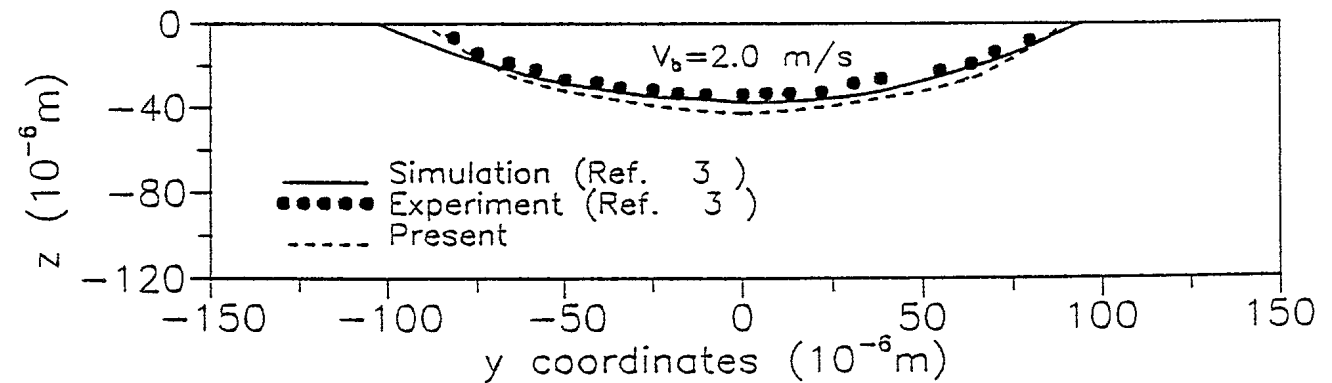
FIGURE 5.3: Dimensionless Maximum Half Depth of the Melted Pool Versus Processing Time



(a)



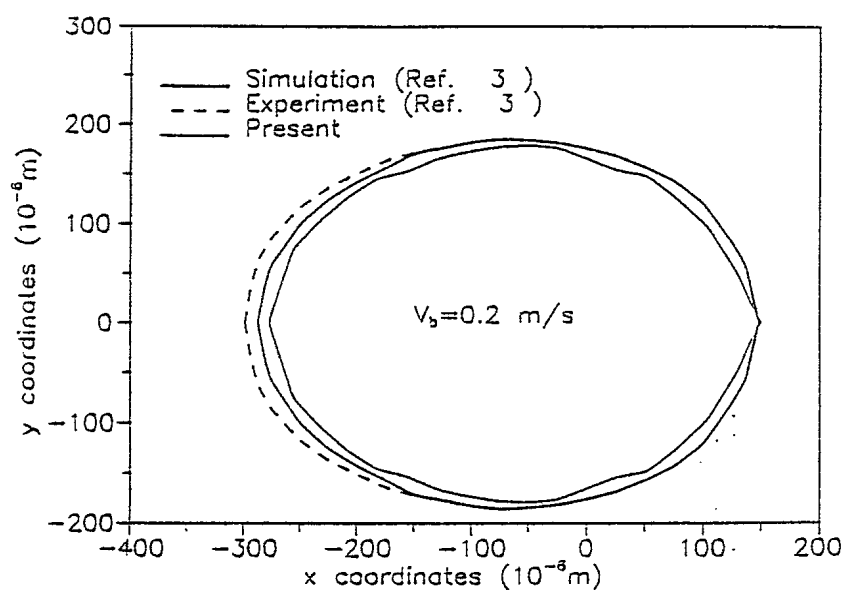
(b)



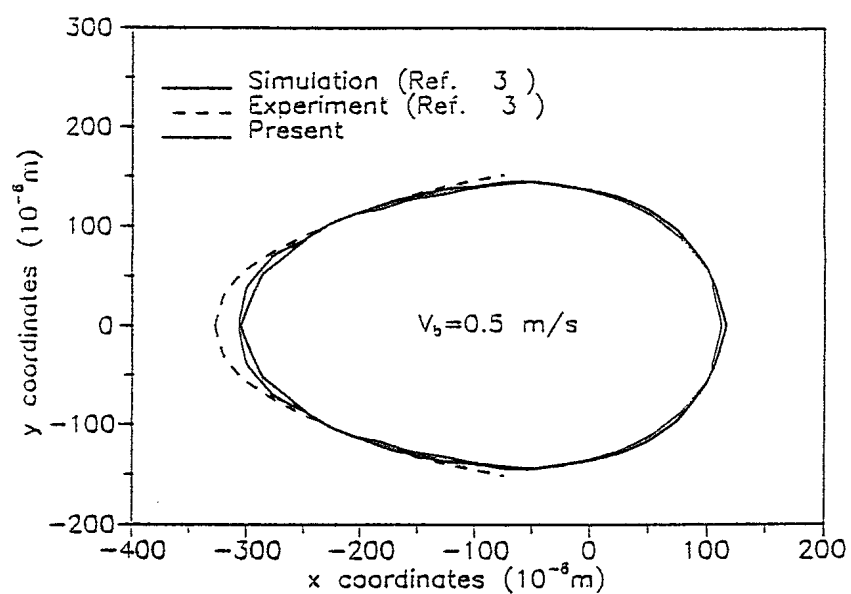
(c)

FIGURE 5.4: Transverse Sectional View of the Remelted Trace for Traversing Velocities of (a) 0.5 m/s, (b) 1.0 m/s and (c) 2.0 m/s

5.10



(a)



(b)

FIGURE 5.5: Top Surface View of the Melted Pool for Traversing Velocities of (a) 0.2 m/s and (b) 0.5 m/s

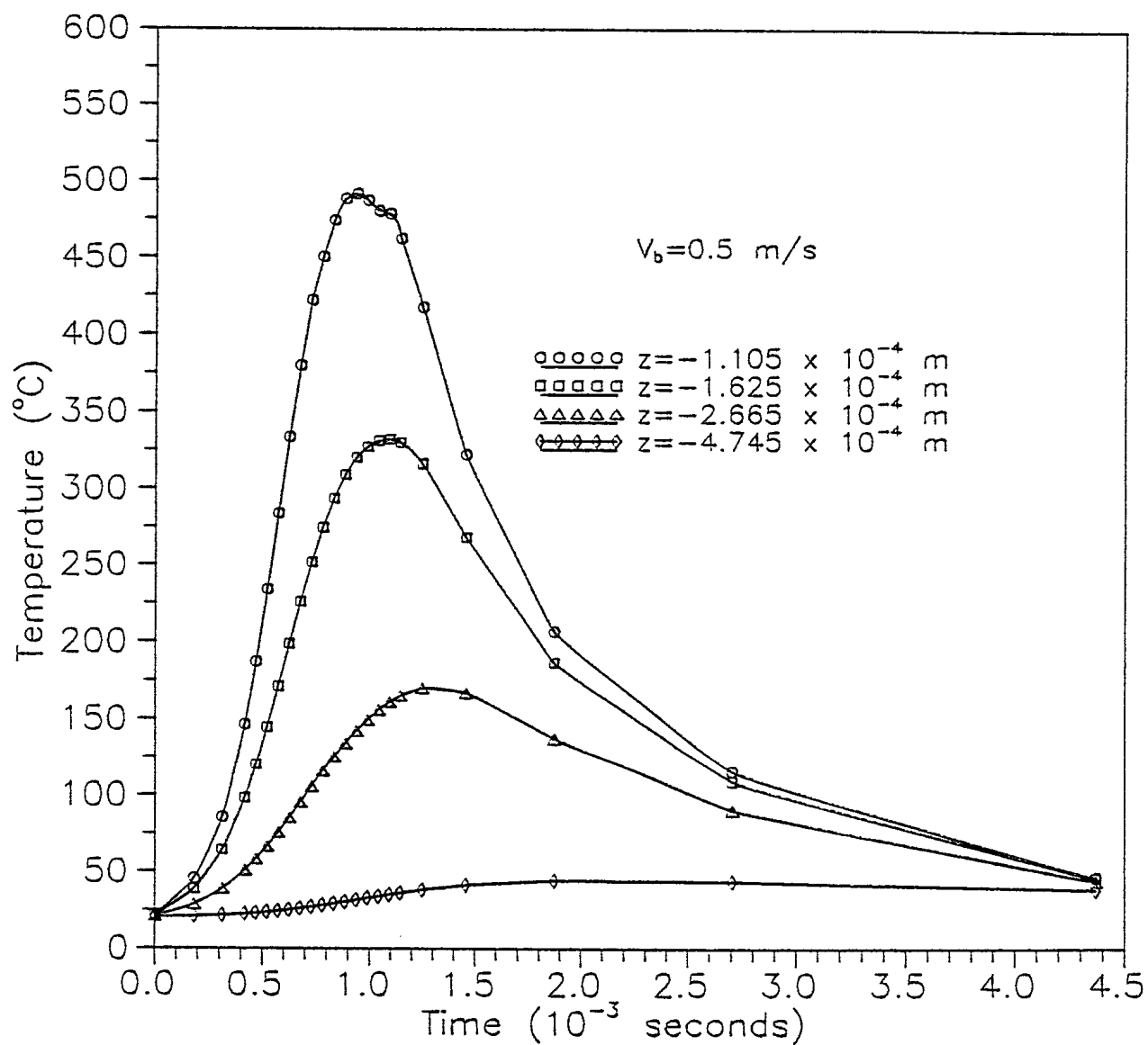
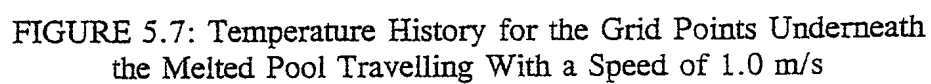


FIGURE 5.6: Temperature History for the Grid Points Underneath the Melted Pool Travelling With a Speed of 0.5 m/s



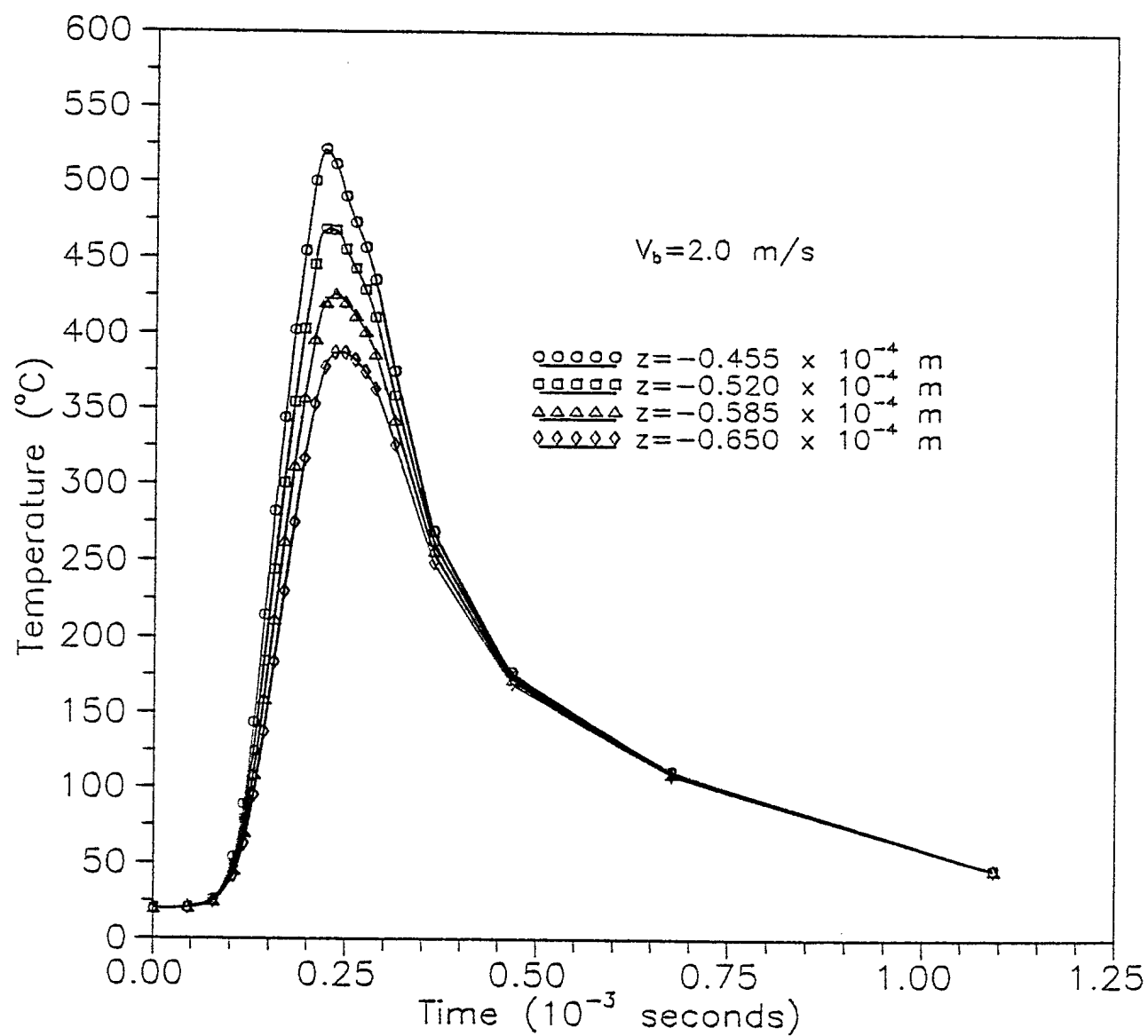


FIGURE 5.8: Temperature History for the Grid Points Underneath the Melted Pool Travelling With a Speed of 2.0 m/s



6. DEVELOPMENT OF GRAPHICAL USER INTERFACE (GUI) FOR THE LASER1 PROGRAM

6.1 Development of the GUI System for LASER1 Program

The graphical user interface (GUI) of the program LASER1 was developed in FORTRAN using the WATCOM FORTRAN compiler. The WATCOM compiler allows a program to interface with Windows API (Application Program Interface) which is part of the Windows SDK (Software Development Kit). The Windows API provides most basic Windows programming functions to facilitate the generation of windows, menus, dialogue boxes, and graphics. It also supports the access to mouse, keyboard, and other I/O devices.

The LASER1 program is a true Windows application, which means it can be executed only within the Windows environment. Its GUI provides a menu-driven system and graphics capability which generates and displays the plots for meshing, laser distribution, and analysis results. The files listed below are related to the LASER1 GUI:

Laserwin.for

This file contains the main driver program and all relevant subroutines to control all the windowing functions, the menu functions and the input functions. The main program also calls the analysis subroutine to perform the analysis when it is requested by the user.

Lasergr.for

This file contains all the graphics subroutines for the provision of mesh plots and post-analysis plots.

Laserwin.rc

This is the resource file. It contains the definitions of windows, menus, and dialogue boxes.

6.2

Laserwin.ico

This is the icon image file.

All these files, besides the analysis routines, are required to create the executable file LASER1.EXE. Detailed descriptions of all GUI functions of the LASER1 program are given in the following sections.

6.2 Description of the GUI System of LASER1 Program

6.2.1 LASER1 GUI Window

The LASER1 program can be run from the file manager of Windows by selecting the file LASER1.EXE and double clicking the mouse. The program will open a new window which has the standard Window system menu and the application menu. Users may resize the window, kill the program, or put the program to background in which case an icon will be displayed.

6.2.2 Menu

The main menu of the LASER1 program contains menu items "File", "Laser", "Material", "Grid", "Analysis", and "Graphics". Some of them have pull-down submenus. The function of each menu item is explained in detail as follows:

"File"

Selection of this item allows the user to either terminate the program or input the prefix of the files which are to be generated or already generated by the program LASER1. A confirmation box is used here to confirm the user's request to exit the program. A submenu is used to allow the users to input the file prefix.

"Laser"

Selection of this item will activate an input dialogue box. Specification of laser input is by means of keyboard entry to each input field. The user can either use the TAB key or mouse to move the cursor between the input fields.

"Material"

This item has a pull-down submenu. There are 11 types of materials whose properties have been predefined in the material database. In addition, there is also a menu item "New material". The selection of this item will activate an input dialogue box by which the user can define the material properties to be used in the analysis. The TAB key or mouse can be used to move the cursor between the input fields.

"Grid"

This item has a pull-down submenu. There are two options for the generation of meshes. The default mesh option generates 23 grid points on X-axis, 15 grid points on Y-axis, and 17 grid points on Z-axis. The mesh will be created by means of these grid points. The "New mesh" option allows the user to input the numbers of grid points on both X-axis and Y/Z-axis using another pull-down submenu. Again, the TAB key or mouse can be used to move the cursor between the input fields.

"Analysis"

Selection of this item is to start the analysis program. A confirmation box is used here to confirm the user's request before actually starting the relatively time-consuming analysis process. After the confirmation, the user will be prompted by a submenu for inputting time increments and maximum allowable time steps. This data is necessary for analysis.

6.4

"Graphics"

This item has a pull-down submenu containing options to plot grid and laser power distribution, temperature contours, melted pool shapes, or temperature time. In these plots, the structure is scaled to fit the graphics window. Necessary information such as dimensions, contour levels, and the depth of melted pool are printed as legends.

For the temperature time history plot, the user can select a point on the side surface by using the left-button of mouse and then plot the temperature time history of that point by clicking the right-button of mouse. It should be noted that only the last selected point is used to compute the time history. The click of left-button of mouse outside the side surface is an invalid point selection and therefore no action will be taken.

6.2.3 Input Data Checking and Program Monitoring

The LASER1 GUI system provides an automated data checking mechanism. In each input dialogue box, after the button "Done" is selected, the completeness of the input data will be checked. If incomplete input data is detected, a warning message will be displayed and the user has the option to correct the problem. If the user wishes to exit any dialogue box without saving newly created input data, the "Cancel" button can be used.

At this point, the analysis is about to be run and a final check on availability of all necessary input data is performed. Again, if the input data is incomplete, a warning message is issued.

The progress of the analysis is monitored by a display of the time step at which the computation is currently being performed. During the analysis, the user may feel that the input devices such as mouse and keyboard are not responding. This is normal because the information from such devices can only be sent to the computer during the next program's I/O action. Therefore, it is advisable that the user does not interrupt the analysis once it is started.

7. A PROPOSED APPROACH FOR ANALYSIS OF HEAT FLOW RESULTING FROM LASER CLADDING WITH A WIRE FEED

7.1 The Physical Model

Some consideration has been given to the potential generalization of the LASER1 program to permit analysis of the laser cladding process. The laser-cladding process is used to deposit a protective layer on a workpiece, and to join the two by a fusion bond. A clad track is obtained by injecting powder particles or by continuously feeding a wire into the melted pool produced by a moving laser beam.

Figure 7.1 shows a longitudinal section view of the laser-affected zone during laser cladding. The laser beam is focused vertically down onto the substrate surface. The wire is fed between the laser beam and the substrate surface and travels simultaneously with the laser beam with a speed v_b . As a result, a part of the substrate surface and the tip of the wire are melted and the melted wire drops on the substrate surface such that a clad track with the thickness of h_c , a fusion bond with the thickness of h_b and a melted pool denoted as Ω_2 are formed.

An Eulerian reference frame which moves with the laser beam is defined, such that the positive x direction coincides with the traversing direction of the laser beam. Hence, the material is moving in the negative direction with a constant velocity, $-v_b$. In Figure 7.1, the origin of the melted pool is located at the point on the original solid substrate surface defining the centre of the laser beam. The boundaries are as follows: Γ_1 is the boundary at which the substrate enters on the right side of the calculation domain, Γ_2 is the top surface including the solid substrate and solid and liquid clad surface, Γ_3 is the "downwind" boundary where both the clad and the substrate leave the calculation domain, and Γ_4 is the boundary at the base of the calculation domain, which may be the surface of the workpiece or an artificial boundary within the base material. The liquid-free surface is defined between the point X_m , the first point of melting, and X_s , the last point on the surface of the clad to solidify.

7.2

7.2 The Governing Equations

Unlike laser melting, the liquid-free surface of the melted pool can no longer be assumed to be flat, but rather is given by a force balance [15] such that

$$-2\mu \frac{\partial v_1}{\partial n} \bar{n} = P_p - P_l + \gamma R \quad (7.1)$$

where P_l is the pressure in the liquid, P_e is the outside pressure, μ is the viscosity, γ is the surface tension coefficient, v_1 is the speed of the fluid flow, and R is the curvature of the clad.

The energy equation for the clad and the substrate in a reference coordinate system attached to the laser beam is given in Reference [15] as:

$$\frac{\partial H}{\partial t} - v_b \frac{\partial H}{\partial x} = \text{div}(k(t) \text{grad}(T)) + Q_l \quad (7.2)$$

where Q_l is a heat sink term in the melted region, which is discussed in Reference [15]. There are two major differences between the laser cladding by powder injection and the laser cladding by wire feeding, from the point of view of simulation. The first is that by powder injection, not all the powders impinged on the substrate surface contribute to the clad or the fusion bond, while by wire feeding all the droplets of the melted wire stay in the clad or in the fusion bond. The second is that the droplets of the melted wire reach the melted pool with a higher temperature ($>$ the liquidus temperature), compared to the powders.

7.3 The Solution Methods

As in laser melting simulations, a finite difference method can be used to discretize Equation (7.2), for the grid points inside the solution domain. The supplementary equations are provided by the boundary conditions [15] on Γ_1 , Γ_2 , Γ_3 and Γ_4 . Thus, once the laser power absorbed by the melted pool, and the curvature of the melted pool surface are known, a steady-state temperature field solution can be obtained through a transient heat transfer

analysis, as carried out in the previous chapters. However, note that the curvature of the melted pool shape, and the relative position of the laser beam are unknown *a priori*. Therefore, the problem of the heat flow resulting from the laser cladding requires a transient and nonlinear analysis. The solution starts by assuming a position of the point X_m relative to the laser beam and the curvature of the liquid-free surface. Following an iterative procedure such as described in Reference [15], the correct position of the point X_m and the curvature of the liquid-free surface can be obtained.

7.4

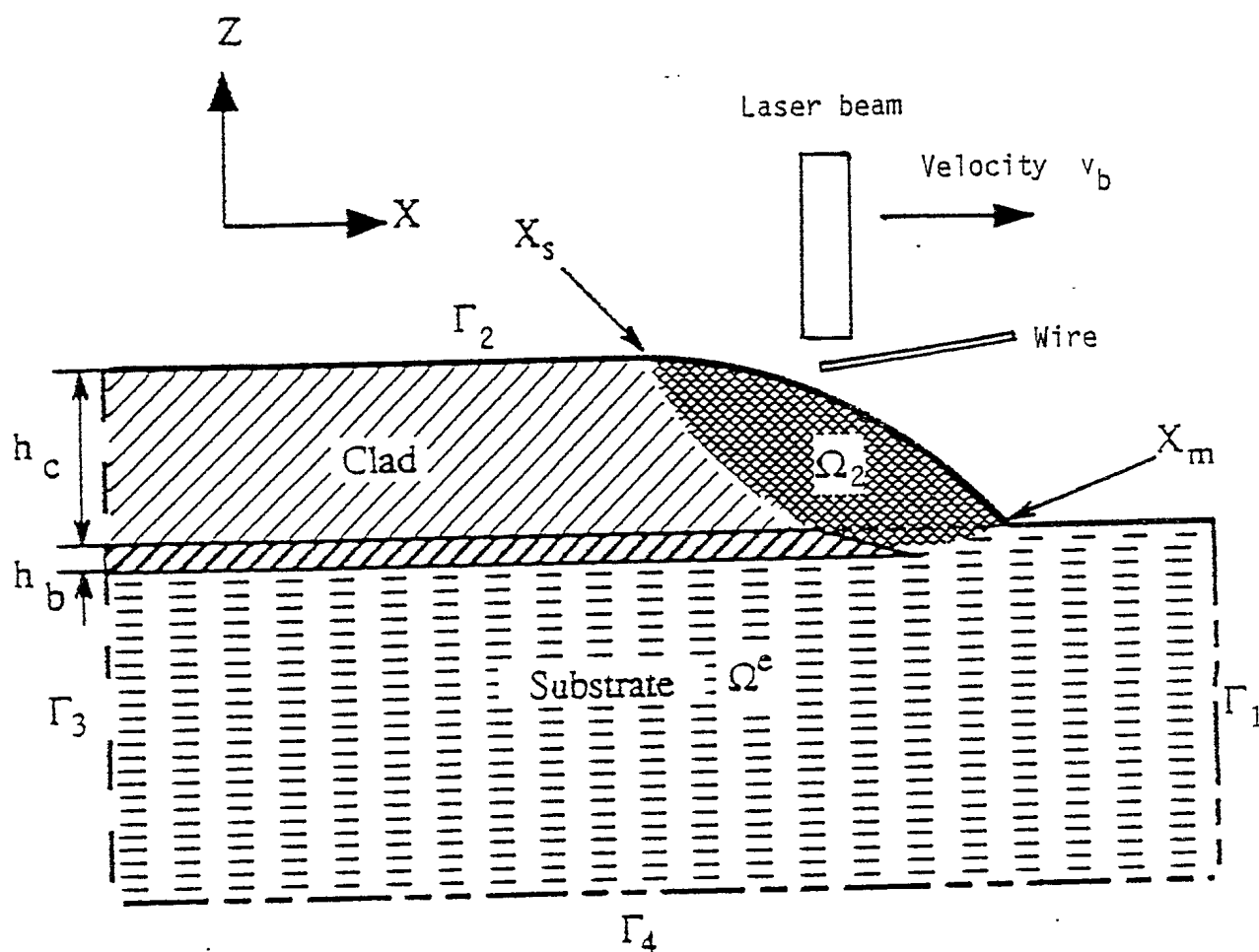


FIGURE 7.1: Process Schematic Showing the Longitudinal Section of the Laser Affected Region During Laser Cladding by a Wire Feed

8. CONCLUSIONS

The aim of this study was to develop a computer program, following the methods given by Hoadley, Rappaz and Zimmermann [3], which would predict the thermal history of the specimen after laser surface treatment with a scanned continuous laser. The LASER1 computer program suite has been developed for this purpose. The program LASER1 was used in this report to simulate the laser surface melting for the eutectic alloy Al-Cu 33 Wt Pct over a range of traversing speeds between 0.2 to 5.0 m/s. Excellent agreement has been obtained between the current simulation results, and the simulation and the experimental results obtained by Hoadley, Rappaz and Zimmermann [3]. In addition, an approach for generalizing LASER1 to permit analysis of the laser cladding process has been outlined.

9. REFERENCES

- [1] C.V. Hyatt, T. Betancourt, and K. MacKay, "Evaluation of Laser Treated Copper Alloys," *Materials Science and Technology*, Vol. 10, pp. 250-255, 1994.
- [2] K. MacKay and C. Hyatt, "The Effect of Laser Surface Modification on the Microstructure of Copper Alloy UNS C3600," *Defence Research Establishment Atlantic Research Note DL/90/2*, 1990.
- [3] A.F.A. Hoadley, M. Rappaz and M. Zimmermann, "Heat-Flow Simulation of Laser Remelting with Experimental Validation," *Metall. Trans. B*, Vol. 22B, pp. 101-109, 1991.
- [4] A.F.A. Hoadley, M. Picasso and M. Rappaz, "Modelling of Solidification Phenomena in Processes Involving a Moving Heat Source," pp. 60-71, Edited by H. Cerjak and K.E. Easterling, "Mathematical Modelling of Weld Phenomena," The Institute of Materials, 1993.
- [5] S. Kou, S.C. Hsu and R. Mehrabian, "Rapid Melting and Solidification of a Surface Due to a Moving Heat Flux," *Metall. Trans. B*, Vol. 12B, pp. 33-45, 1981.
- [6] S. Kou and Y.H. Wang, "Three-Dimensional Convection in Laser Melted Pools," *Metall. Trans. A*, Vol. 17A, pp. 2265-2270, 1986.
- [7] A. Paul and T. Debroy, "Free Surface Flow and Heat Transfer in Conduction Mode Laser Welding," *Metall. Trans. B*, Vol. 19B, pp. 851-858, 1988.
- [8] T. Zacharia, S.A. David, J.M. Vitek and T. Debroy, "Heat Transfer during Nd:Yag Pulsed Laser Welding and Its Effect on Solidification Structure of Austenitic Stainless Steels," *Metall. Trans. A*, Vol. 20A, pp. 957-967, 1989.
- [9] N. Ramanan and S. A. Korpela, "Fluid Dynamics of a Stationary Weld Pool," *Metall. Trans. A*, Vol. 21A, pp. 45-57, 1990.
- [10] T. Chande and J. Mazumder, "Estimating Effects of Processing Conditions and Variable Properties up on Pool Shape, Cooling Rates, and Absorption Coefficient in Laser Welding," *J. Appl. Physics*, Vol. 56, pp. 1981-1986, 1984.
- [11] C.L. Chan, R. Zehr, J. Mazumder and M.M. Chen, "Three-Dimensional Model for Convection in Laser Weld Pool," pp. 229-246, *Modelling and Control of Casting and Welding Processes*, TMS, Warrendale, PA, 1986.

9.2

- [12] J.A. Hopkins, T.D. McCay, M.H. McCay and A.H. Eraslan, "Modelling of Laser Welding: Comparison of 1-g and μ -g Predictions," pp. 17-24, in "Transport Phenomena in Non-conventional Manufacturing and Materials Processing," HTD-Vol. 259, ASME, New York, 1993.
- [13] M. Zimmermann, M. Carrard and W. Kurz "Rapid Solidification of Al-Cu Eutectic Alloy by Laser Remelting," *Acta Metall.*, Vol. 37, pp. 3305-3313, 1989.
- [14] A. Frenk, A.F.A. Hoadley and J.-D. Wagniere, "In-Situ Technique for Measuring the Absorption during Laser Remelting," *Metall. Trans. B*, Vol. 22B, pp. 139-141, 1991.
- [15] A.F.A. Hoadley and M. Rappaz, "A Thermal Model of Laser Cladding by Powder Injection," *Metall. Trans. B*, Vol. 23B, pp. 631-642, 1991.
- [16] M. Picasso, C.F. Marsden, J.-D Wagniere, A. Frenk, and M. Rappaz, "A Simple but Realistic Model for Laser Cladding," *Metall. Trans. B*, Vol. 25B, pp. 281-291, 1994.
- [17] M. Picasso and M. Rappaz, "Laser-Powder-Material Interactions in the Laser Cladding Process," *Journal De Physique IV*, Vol. 4, pp. C4-27 - C4-33, 1994.
- [18] Y. Liu, J. Koch, J. Mazumder and K. Shibata, "Processing, Microstructure, and Properties of Laser-Clad Ni Alloy FP-5 on Al Alloy AA333," *Metall. Trans. B*, Vol. 25B, pp. 425-434, 1994.
- [19] Y. Liu, J. Mazumder and K. Shibata, "Laser Cladding of Ni-Al Bronze on Al Alloy AA333," *Metall. Trans. B*, Vol. 25B, pp. 749-759, 1994.
- [20] F. Thomasset, "Implementation of Finite Element Methods for Navier-Stokes Equations," Springer-Verlag, New York, pp. 37-40, 1981.
- [21] J.F. Lancaster, "Metallurgy of Welding," George Allen & Unwin, London, p. 42, 1980.
- [22] J.P. Holman, "Heat Transfer," Sixth Edition, McGraw-Hill, New York, 1986.
- [23] G.E. Myers, "Analytical Methods in Conduction Heat Transfer," Genium Publishing Corporation, Schenectady, NY, 1987.
- [24] W.W. Hager, "Applied Numerical Linear Algebra," Prentice Hall, Englewood Cliffs, New Jersey, 1988.
- [25] M. Gunduz and J.D. Hunt, "The Measurement of Solid-Liquid Surface Energies in the Al-Cu, Al-Si and Pb-Sn Systems," *Acta Metall.*, Vol. 33, pp. 1651-1672, 1985.

- [26] M.C. Flemings, "Solidification Processing," McGraw-Hill, New York, 1974.
- [27] C.V. Hyatt, "Thermochemical and Optical Data for Use in Finite Difference Heat Transfer Program to Model Laser Surface Melting," DREA Technical Note, 1995.

APPENDIX A:
THERMOCHEMICAL AND OPTICAL DATA FOR ALUMINUM BRONZES,
COPPER NICKEL ALLOYS AND GUN STEELS



THERMOCHEMICAL AND OPTICAL DATA FOR ALUMINUM BRONZES, COPPER NICKEL ALLOYS AND GUN STEELS

To make the program LASER1 convenient to use for the materials of interest in DREA's laser surface engineering research, such as aluminum bronzes, copper nickel alloys and gun steels, data for these materials has been included in the program in the form of lookup tables. Thus, for simulations involving those materials, the user does not need to look up and input material properties. These materials are defined in the material menu in the program LASER1, and consist of eutectic alloy Al-Cu 33 Wt Pct, aluminum alloy AISI 2024, steel AISI 1025, stainless steel AISI 304, nickel aluminum bronze UNS C95800, copper nickel alloys containing 1, 3, 5, 10, 20 and 30 weight % nickel. The thermochemical and optical data for all the materials except Al-Cu 33 Wt Pct were provided by DREA [27]. The sources of the material data and the assumptions made are outlined in Reference 27. To comply with the linear function of temperature assumptions made in the program LASER1 for the input data, further simplification has been made for the thermal conductivity and the thermal specific heat of steel AISI 1025 and of stainless steel AISI 304. Tables A.1 to Table A.10 contains these data used in the program.

A.2

TABLE A.1: Thermophysical Data for Aluminum Alloy AISI 2024	
Solidus temperature	502°C
Liquidus temperature	638°C
Surface absorption (solid)	$9.5 + 6.3 \times 10^{-3}T$ Pct
Surface absorption (liquid)	40 Pct
Density	2770 kg/m ³
Specific heat (solid)	2.42×10^6 J/m ³ °C
Specific heat (liquid)	2.42×10^6 J/m ³ °C
Latent heat	1.09×10^7 J/m ³
Thermal conductivity (solid)	120 W/m/°C
Thermal conductivity (liquid)	120 W/m/°C

TABLE A.2: Thermophysical Data for Steel AISI 1025	
Solidus temperature	1470°C
Liquidus temperature	1520°C
Surface absorption (solid)	12 Pct
Surface absorption (liquid)	40 Pct
Density	7850 kg/m ³
Specific heat (solid)	$4.1 \times 10^6 + 1.52 \times 10^3 T$
Specific heat (liquid)	6.42×10^6 J/m ³ °C
Latent heat	2.12×10^9 J/m ³
Thermal conductivity (solid)	$52.5 - 1.39 \times 10^{-2}T$ W/m/°C
Thermal conductivity (liquid)	35 W/m/°C

A.3

TABLE A.3: Thermophysical Data for Stainless Steel AISI 304	
Solidus temperature	1400°C
Liquidus temperature	1420°C
Surface absorption (solid)	12 Pct
Surface absorption (liquid)	40 Pct
Density	8000 kg/m ³
Specific heat (solid)	$3.22 \times 10^6 + 1.44 \times 10^3 T$ J/-m ³ °C
Specific heat (liquid)	6.42×10^6 J/m ³ °C
Latent heat	2.12×10^9 J/m ³
Thermal conductivity (solid)	$12.91 + 1.88 \times 10^{-2} T$ W/m/°C
Thermal conductivity (liquid)	35 W/m/°C

TABLE A.4: Thermophysical Data for Nickel Aluminum Bronze UNS C95800	
Solidus temperature	1045°C
Liquidus temperature	1060°C
Surface absorption (solid)	12 Pct
Surface absorption (liquid)	40 Pct
Density	7640 kg/m ³
Specific heat (solid)	4.03×10^6 J/m ³ °C
Specific heat (liquid)	4.03×10^6 J/m ³ °C
Latent heat	1.75×10^9 J/m ³
Thermal conductivity (solid)	36 W/m/°C
Thermal conductivity (liquid)	36 W/m/°C

A.4

TABLE A.5: Thermophysical Data for Copper Nickel Alloy Cu-1w%Ni	
Solidus temperature	1090°C
Liquidus temperature	1091°C
Surface absorption (solid)	12 Pct
Surface absorption (liquid)	40 Pct
Density	8940 kg/m ³
Specific heat (solid)	3.43x10 ⁶ J/m ³ °C
Specific heat (liquid)	3.43x10 ⁶ J/m ³ °C
Latent heat	1.92x10 ⁹ J/m ³
Thermal conductivity (solid)	64 W/m/°C
Thermal conductivity (liquid)	64 W/m/°C

TABLE A.6: Thermophysical Data for Copper Nickel Alloy Cu-3w%Ni	
Solidus temperature	1095°C
Liquidus temperature	1121°C
Surface absorption (solid)	12 Pct
Surface absorption (liquid)	40 Pct
Density	8940 kg/m ³
Specific heat (solid)	3.41x10 ⁶ J/m ³ °C
Specific heat (liquid)	3.41x10 ⁶ J/m ³ °C
Latent heat	1.92x10 ⁹ J/m ³
Thermal conductivity (solid)	60 W/m/°C
Thermal conductivity (liquid)	60 W/m/°C

TABLE A.7: Thermophysical Data for Copper Nickel Alloy Cu-5w%Ni	
Solidus temperature	1100°C
Liquidus temperature	1127°C
Surface absorption (solid)	12 Pct
Surface absorption (liquid)	40 Pct
Density	8940 kg/m ³
Specific heat (solid)	3.40x10 ⁶ J/m ³ °C
Specific heat (liquid)	3.40x10 ⁶ J/m ³ °C
Latent heat	1.92x10 ⁹ J/m ³
Thermal conductivity (solid)	55 W/m/°C
Thermal conductivity (liquid)	55 W/m/°C

TABLE A.8: Thermophysical Data for Copper Nickel Alloy Cu-10w%Ni (UNS C70600)	
Solidus temperature	1100°C
Liquidus temperature	1150°C
Surface absorption (solid)	12 Pct
Surface absorption (liquid)	40 Pct
Density	8940 kg/m ³
Specific heat (solid)	3.40x10 ⁶ J/m ³ °C
Specific heat (liquid)	3.40x10 ⁶ J/m ³ °C
Latent heat	1.98x10 ⁹ J/m ³
Thermal conductivity (solid)	42 W/m/°C
Thermal conductivity (liquid)	42 W/m/°C

A.6

TABLE A.9: Thermophysical Data for Copper Nickel Alloy Cu-20w%Ni (UNS C7100)	
Solidus temperature	1150°C
Liquidus temperature	1200°C
Surface absorption (solid)	12 Pct
Surface absorption (liquid)	40 Pct
Density	8940 kg/m ³
Specific heat (solid)	3.40x10 ⁶ J/m ³ °C
Specific heat (liquid)	3.40x10 ⁶ J/m ³ °C
Latent heat	2.04x10 ⁹ J/m ³
Thermal conductivity (solid)	36 W/m/°C
Thermal conductivity (liquid)	36 W/m/°C

TABLE A.10: Thermophysical Data for Copper Nickel Alloy Cu-30w%Ni (UNS C71500)	
Solidus temperature	1170°C
Liquidus temperature	1240°C
Surface absorption (solid)	12 Pct
Surface absorption (liquid)	40 Pct
Density	8940 kg/m ³
Specific heat (solid)	3.40x10 ⁶ J/m ³ °C
Specific heat (liquid)	3.40x10 ⁶ J/m ³ °C
Latent heat	2.13x10 ⁹ J/m ³
Thermal conductivity (solid)	29 W/m/°C
Thermal conductivity (liquid)	29 W/m/°C

APPENDIX B:
USER'S GUIDE FOR THE PROGRAM LASER1



USER'S GUIDE FOR THE PROGRAM LASER1

B1. Computer System Requirements

The LASER1 program is a true Windows application which means it can be executed only within the Windows environment. The computer system requirements are a minimum 486-PC with 16 MB RAM and a MS Windows operating system.

B2. Getting Started

The LASER1 program can be run from the file manager of Windows by selecting the file LASER1.EXE and double clicking with the mouse. The program will open a new window which has the standard windows system menu and the application menu, as shown in Figure B.1 and this window is referred to as the main menu. There are three possible options by which to proceed. The first option perhaps is to exit the program LASER1. This can be carried out by clicking on the item "File" and clicking on the item "Exit" in the submenu prompt, shown in Figure B.2. The second option is to display or review the results obtained from a completed analysis. This is achieved by clicking on the item "File" to input the prefix of the files and clicking on the item "Graphics" to start displaying results. The third option is to start a new analysis. In the following sections, the last two options are explained step by step. It should be mentioned that the data entry is insensitive to the use of integer or real number formats.

B3. Starting New Analysis

For this purpose four steps are required:

- a. Name a five-character prefix for the files which will be generated by the program LASER1 by clicking on the item "File" in the main menu shown in Figure B.1. This

B.2

is achieved by clicking on the item "File Prefix" in the submenu prompt, shown in Figure B.2, and entering five characters in the next submenu prompt, shown in Figure B.3, and confirming the input;

- b. Input the laser-related data by first clicking on the item "LASER" within the main menu and then entering the data as required by the submenu prompt, as shown in Figure B.4. In this submenu, starting from the top, the first data entry relates to the laser power distribution, which is either equal to 1 (the Gaussian distribution) or equal to 2 (the uniform distribution); the second data entry is the laser power in unit of Watts (W); the third data entry is the laser focal diameter in unit of meters (m); the fourth data entry is the traverse velocity of the laser beam in unit of m/sec; the fifth data entry is the ambient temperature ($^{\circ}\text{C}$); the last data entry is the surface heat-transfer coefficient ($\text{W}/\text{m}^2/^{\circ}\text{C}$);
- c. Input the material-related data by first clicking on the item "Material" within the main menu and then selecting one of the materials in the library or inputting each material parameter required by the program. If the material which the user wishes to use is among 11 materials shown in the submenu prompted, as shown in Figure B.5, this step is completed by clicking on the name of the material. These default materials are:

- Steel AISI 1025
- Stainless steel AISI 304
- Aluminum alloy AISI 2024
- Eutectic alloy AL-CU 33 Wt Pct
- Copper nickel alloy Cu-1 w% Ni
- Copper nickel alloy Cu-3 w% Ni
- Copper nickel alloy Cu-5 w% Ni
- Copper nickel alloy Cu-10 w% Ni (UNS C70600)
- Copper nickel alloy Cu-20 w% Ni (UNS C71000)
- Copper nickel alloy Cu-30 w% Ni (UNS C71500)
- Nickel aluminum bronze (UNS C95800).

Otherwise, the users should click on the item "New Material" to obtain the submenu shown in Figure B.6 for entry of the material data into the program. There are 15 data entries requested in this submenu. Starting from the top, the first entry is the solidus temperature ($^{\circ}\text{C}$); the second is the liquidus temperature ($^{\circ}\text{C}$); the third entry is the equilibrium partition ratio (the current version of the program ignores this data, so the users can enter any number for this); the fourth entry and the fifth entry are the constants A and B, for the surface absorption rate of the solid surface, expressed as the form $(A+BT)\%$, respectively; the sixth entry is the liquid surface absorption rate (%); the seventh entry is the density (kg/m^3); the eighth and the ninth entries are the constants A and B for the specific heat of the solid material expressed as the form $(A+BT)\%$ with the unit of $\text{J}/^{\circ}\text{C}/\text{m}^3$, respectively; the tenth entry is the specific heat

of the liquid material ($\text{J}/^\circ\text{C}/\text{m}^3$); the eleventh entry is the latent heat (J/m^3); the twelfth and thirteenth entries are the constants A and B for the thermal conductivity of the material in the solid state, expressed as the form $(A+BT)$ in unit of $\text{W}/\text{m}/^\circ\text{C}$, respectively; the fourteenth entry is the thermal conductivity of the material in the liquid state ($\text{W}/\text{m}/^\circ\text{C}$); the last entry is the average thermal diffusivity of the material (m^2/s); if this entry is entered as zero, the program computes the average thermal diffusivity;

- d. Input the grid-related data by first clicking on either the item "Default Mesh" or the item "New Mesh" in the submenu shown in Figure B.7. If the item "Default Mesh" is clicked, this step is completed and there will be 23 grid points in X-direction, 15 grid points in Y-direction and 17 grid points in Z-direction, when generating the finite difference grid, with respect to the coordinate system shown in Figure 2.1. If the item "New Mesh" is clicked, a submenu shown in Figure B.8 will be prompted and the users are requested to enter two data quantities into this submenu. Starting from the top, the first entry is the number of grid points on X-axis, with respect to the coordinate system shown in Figure 2.1, used to generate the finite difference grid; the second entry is the number of grid points on Y- or Z-axis. For a computer with 16 MB RAM, the grid points on X-axis should be less than 24, the grid points on Y/Z-axis should be less than 17. This step is completed after confirming the entries are correct; and
- e. The fifth and last step, is to initiate the analysis by clicking on the item "Analysis" in the main menu. This will produce the dialogue box shown in Figure B.9 which serves to confirm the user's request before actually starting the relatively time-consuming analysis process. After the confirmation, the user will be prompted with a submenu as shown in Figure B.10, for inputting time increments and the maximum allowable time steps. The default time increment and the default maximum allowable time steps are 0.1 and 100, respectively. After confirming the entries, the program will perform the analysis. A small box will appear in the centre of the main menu to inform the user of the status of analysis. When the analysis has been completed, this box together with the main menu, takes the form shown in Figure B.11.

B4. Displaying of Results

The results can be displayed by first clicking on the item "Graphics" in the main menu. This will produce the submenu shown in Figure B.12. There are seven sets of results which can be displayed.

B.4

- i. The first set of results is the grid and the laser power distribution and it is displayed by clicking on the item "Grid and Laser Distribution" in the submenu. The output typically looks like that shown in Figure B.13;
- ii. The second set of the results is the three-dimensional temperature contour for the model and is displayed by clicking on the item "3D Contour". Typically, these results are shown in Figure B.14;
- iii. The third set of the results is the temperature contour plot on the top surface of the model and it is displayed by clicking on the item "Top Surface Contour". The result is similar to that shown in Figure B.15;
- iv. The fourth set of the results is the temperature contour plot on the centre plane, i.e. the symmetrical plane with $Y=0$ as defined in Figure 2.1, and it is displayed by clicking on the item "Centre Plane Contour". The result looks like that shown in Figure B.16;
- v. The fifth set of the results is the plan view of the melt-pool intersection with the top surface and it is displayed by clicking on the item "Melt Pool Surface Shape". The result looks like that shown in Figure B.17;
- vi. The sixth set of the results is the side view of the melt-pool intersected with the centre plane, i.e. the plane with $Y=0$, and it is displayed by clicking on the item "Melt Pool Transverse Shape". The result looks like that shown in Figure B.18;
- vii. The seventh set of the results is the temperature time history plot for a user selected point and it is displayed by first clicking on the item "Temperature Time History". This will prompt a window containing a transverse view of the melt pool as shown in Figure B.19a. With the appearance of the cursor, the user is expected to use the left mouse button to select a point and then press the right mouse button to activate the program. This will bring up the final result which may look similar to that shown in Figure B.19b.

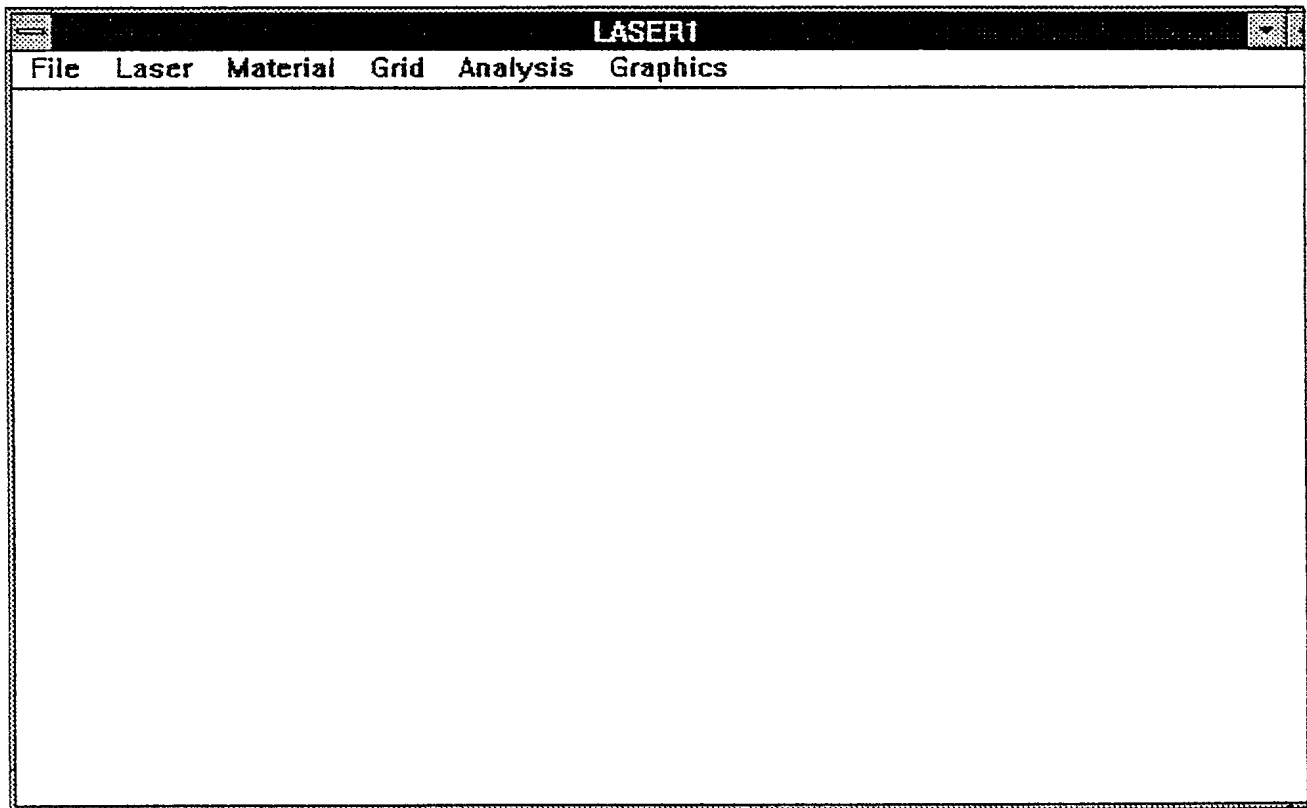


FIGURE B.1: Main Menu of the Program LASER1

B.6

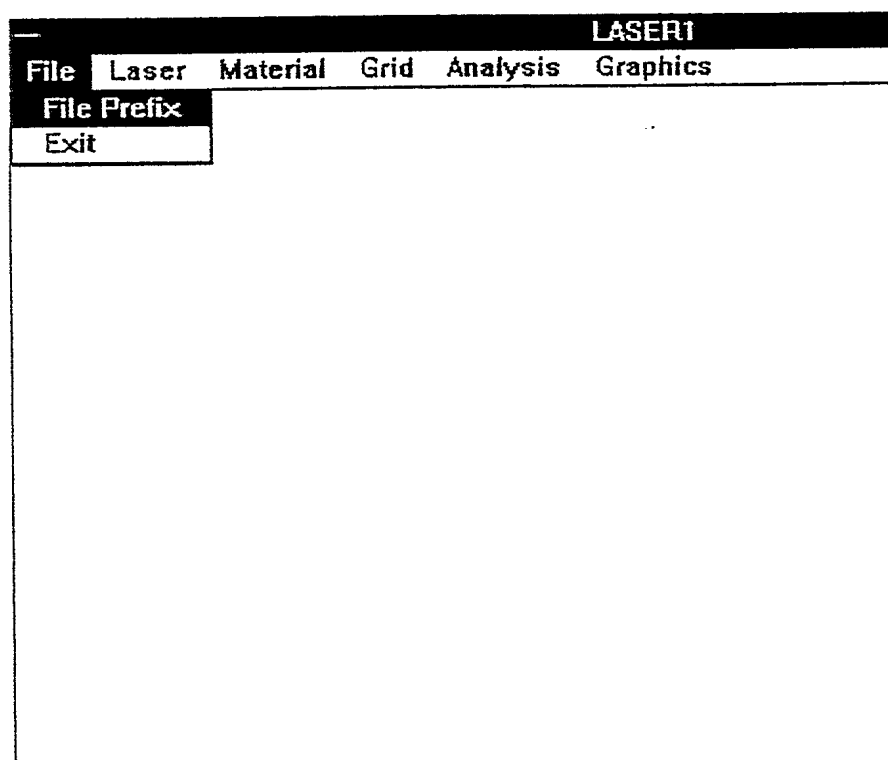
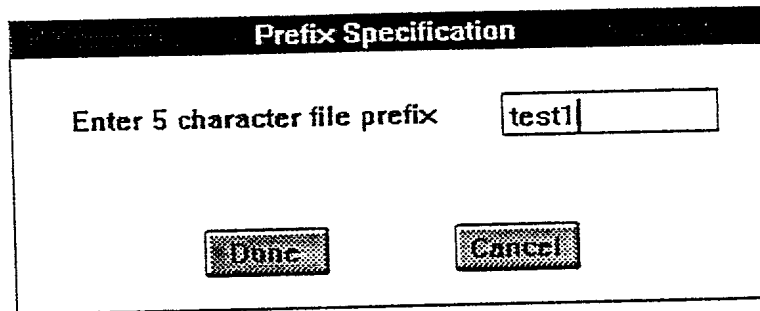


FIGURE B.2: The Submenu Prompt Following the Selection of the Item "File" in the Main Menu

B.7



A screenshot of a software dialog box titled "Prefix Specification". The dialog box has a black title bar with the text "Prefix Specification" in white. Below the title bar, the text "Enter 5 character file prefix" is displayed. To the right of this text is a text input field containing the text "test1". Below the input field, there are two buttons: "Done" and "Cancel".

FIGURE B.3: The Submenu Prompt Following the Selection of the Item "File Prefix" in the Main Menu

B.8

Laser Specification	
Distribution [1=Gaussian, 2=Uniform]	<input type="text"/>
Laser Power [W]	<input type="text"/>
Focal Diameter [m]	<input type="text"/>
Traverse Velocity [m/s]	<input type="text"/>
Ambient Temperature [C]	<input type="text"/>
Surface HTC [W/C/m/m]	<input type="text"/>
<div><input type="button" value="Done"/> <input type="button" value="Cancel"/></div>	

FIGURE B.4: The Submenu Prompt Following the Selection of the Item "Laser" in the Main Menu

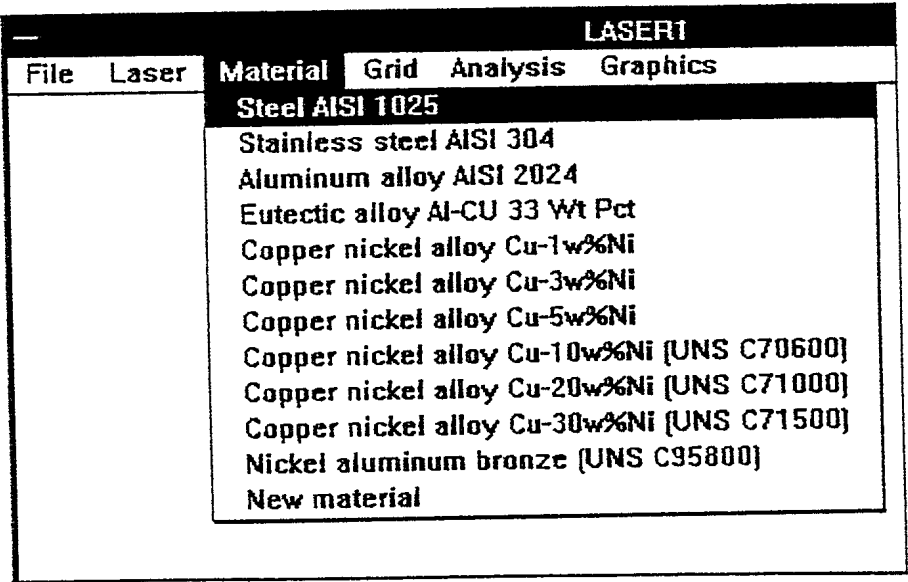


FIGURE B.5: The Submenu Prompt Following the Selection of the Item "Material" in the Main Menu

B.10

Material Specification

Solidus Temperature [C]	
Liquidus Temperature [C]	
Equilibrium Partition Ratio [=<1]	
Surface Absorption [solid, %], Constant A	
A + BT, Constant B	
Surface Absorption [liquid, %]	
Density [Kg/m3]	
Specific Heat [solid], Constant A	
A + BT, [J/C/m3] Constant B	
Specific Heat [liquid, J/C/m3]	
Latent Heat [J/m3]	
Thermal Conductivity [solid], Constant A	
A + BT, [W/m/C] Constant B	
Thermal Conductivity [liquid, W/m/C]	
Average Thermal Diffusivity [m2/S]	

Done

Cancel

FIGURE B.6: The Submenu Prompt Following the Selection of the Item "New Material" in the Main Menu

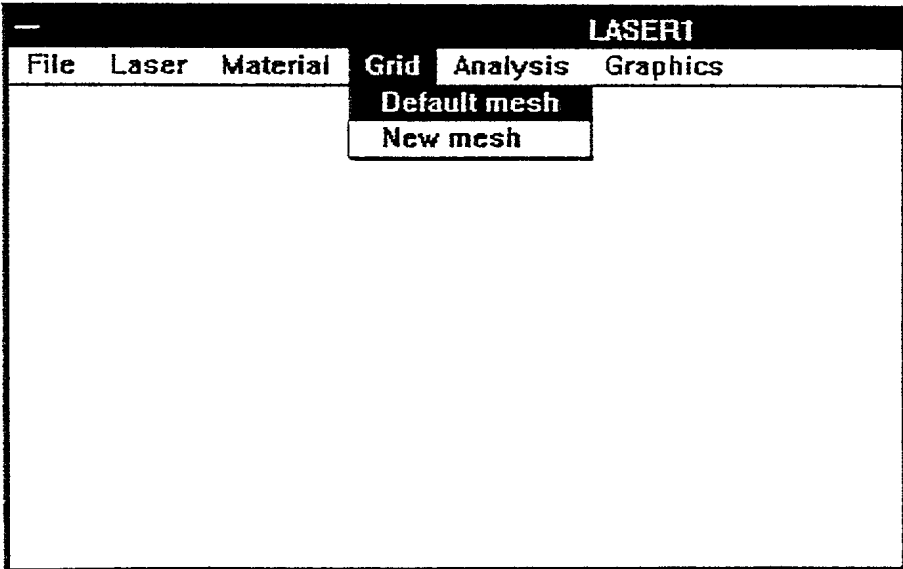
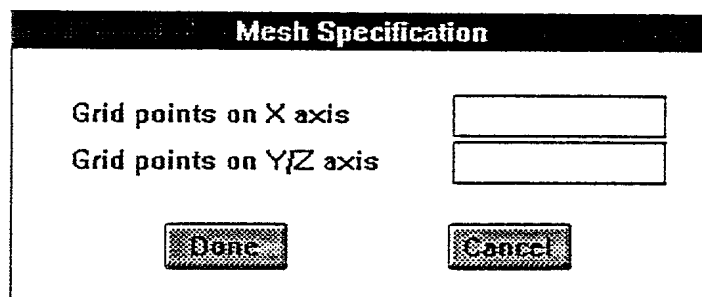


FIGURE B.7: The Submenu Prompt Following the Selection of the Item "Grid" in the Main Menu

B.12



The image shows a dialog box titled "Mesh Specification". It contains two input fields: "Grid points on X axis" and "Grid points on Y/Z axis". Below these fields are two buttons: "Done" and "Cancel".

Mesh Specification	
Grid points on X axis	<input type="text"/>
Grid points on Y/Z axis	<input type="text"/>
<input type="button" value="Done"/>	<input type="button" value="Cancel"/>

FIGURE B.8: The Submenu Prompt Following the Selection of the Item "New Mesh" in the Main Menu

B.13

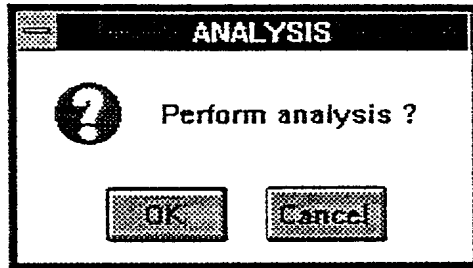
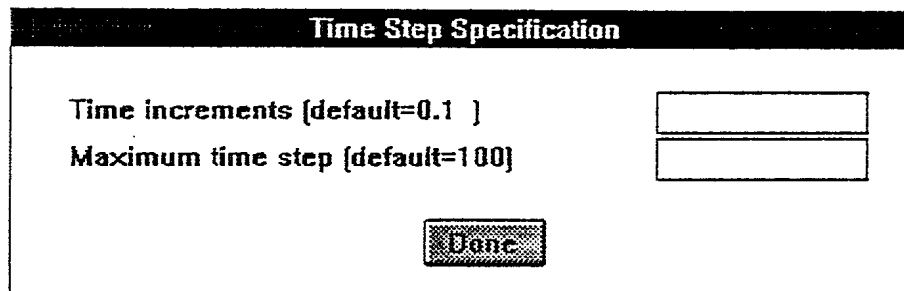


FIGURE B.9: The Dialogue Box Prompt Following the Selection of the Item "Analysis" in the Main Menu

B.14



The image shows a software dialog box titled "Time Step Specification". It contains two input fields: "Time increments (default=0.1)" and "Maximum time step (default=100)". Both fields are currently empty. Below the input fields is a "Done" button.

Time Step Specification	
Time increments (default=0.1)	<input type="text"/>
Maximum time step (default=100)	<input type="text"/>
<input type="button" value="Done"/>	

FIGURE B.10: The Submenu to Confirm the Start of the Analysis

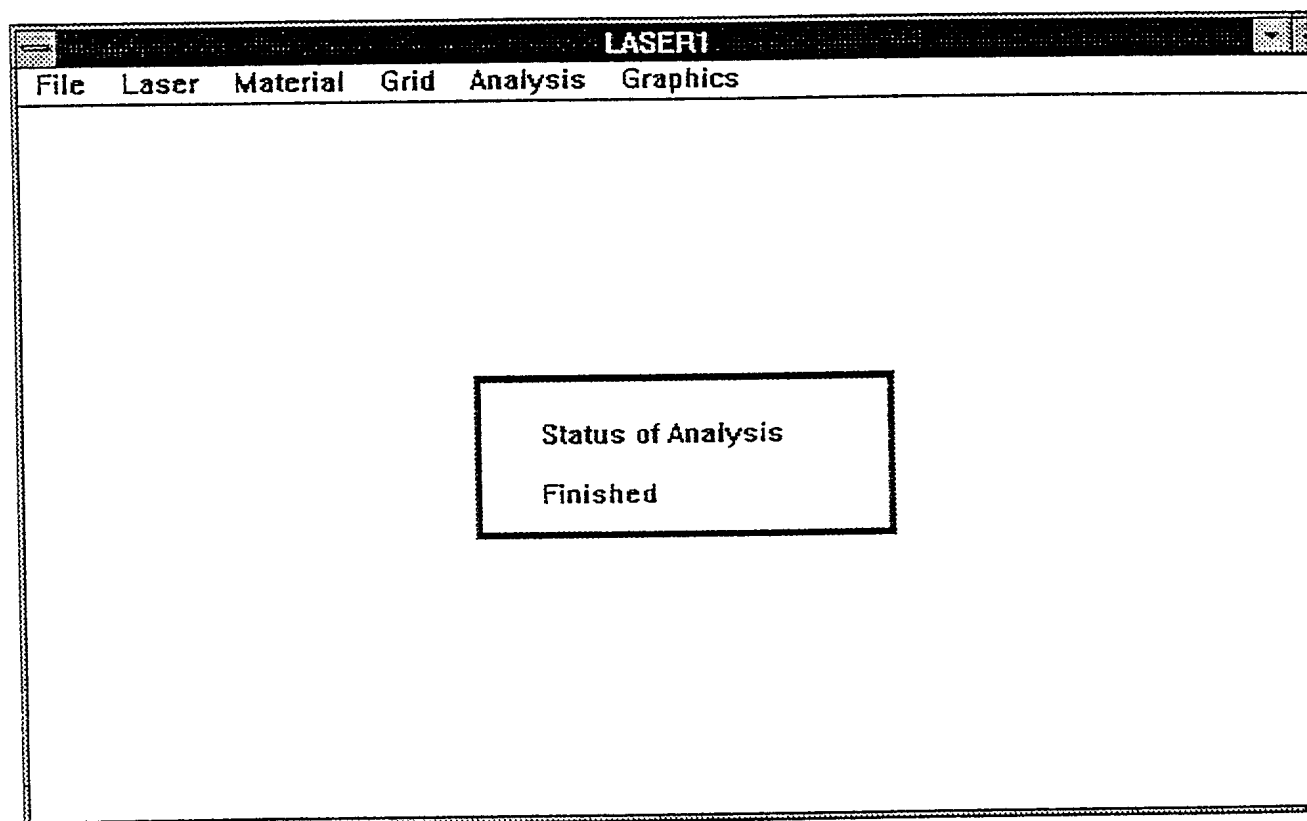


FIGURE B.11: The Main Menu Following Analysis Completion

B.16

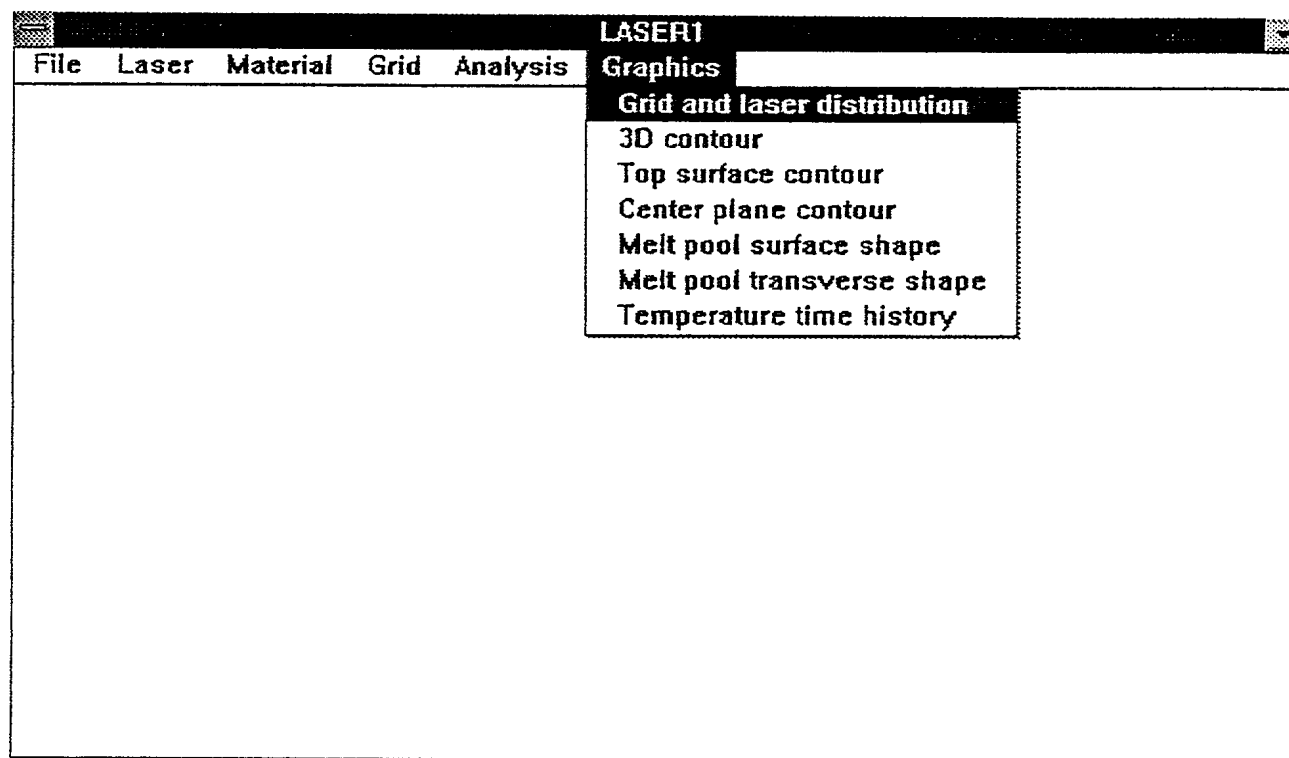


FIGURE B.12: The Submenu Prompt Following the Selection of the Item "Graphics" in the Main Menu

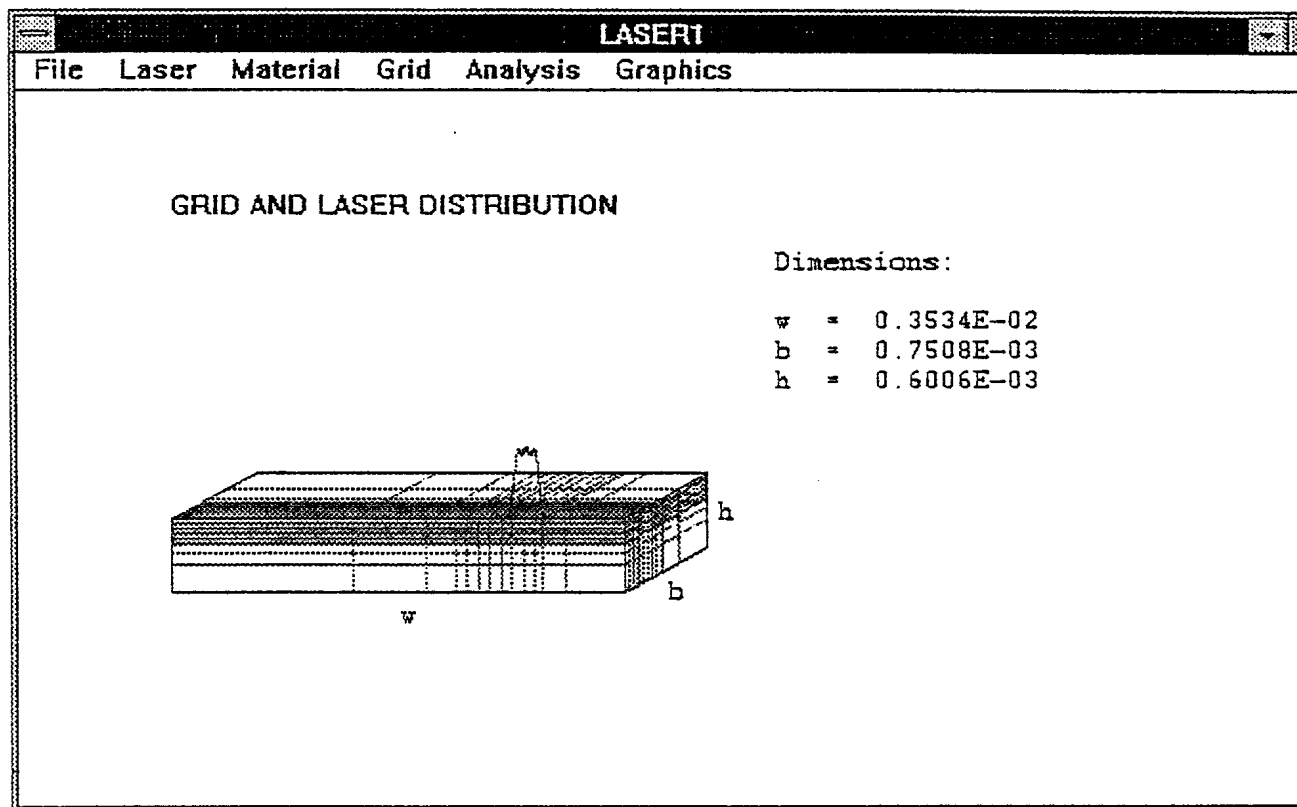


FIGURE B.13: Grid and Laser Power Distributions

B.18

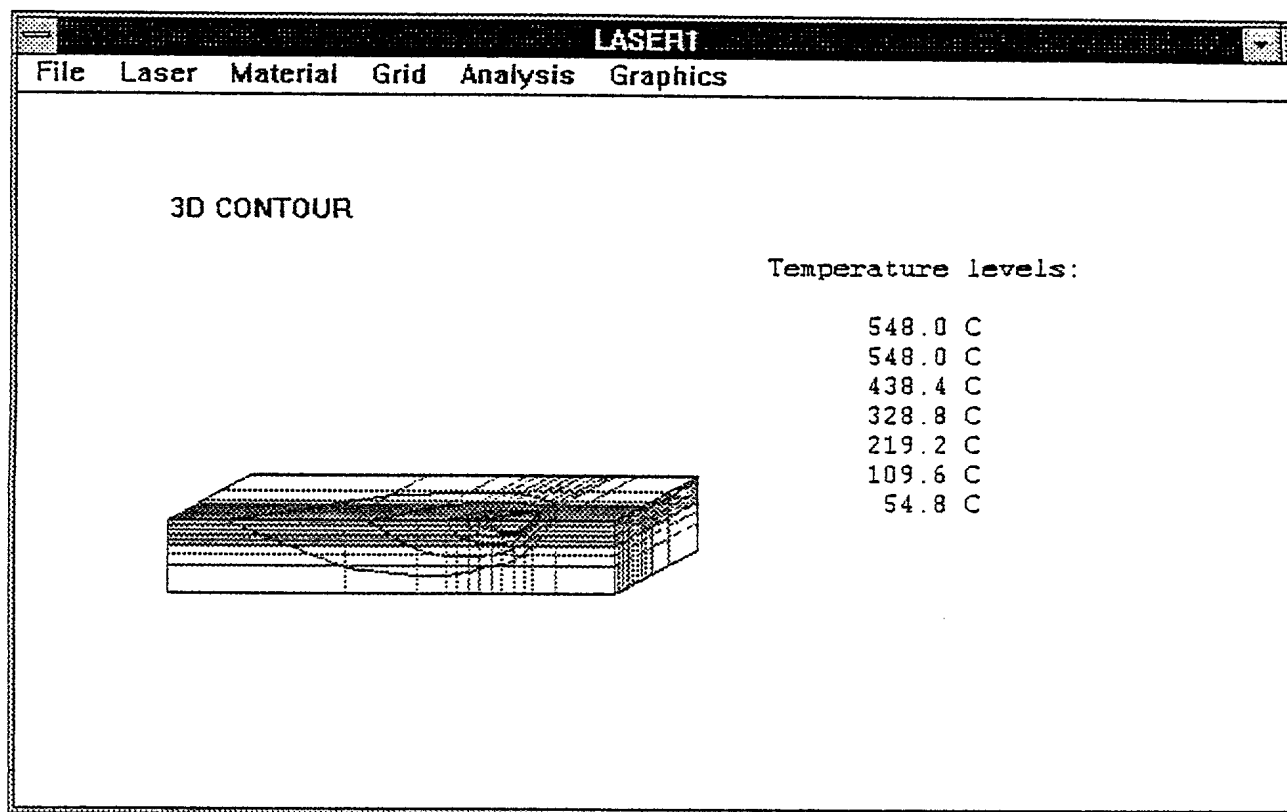


FIGURE B.14: 3-D Temperature Contours

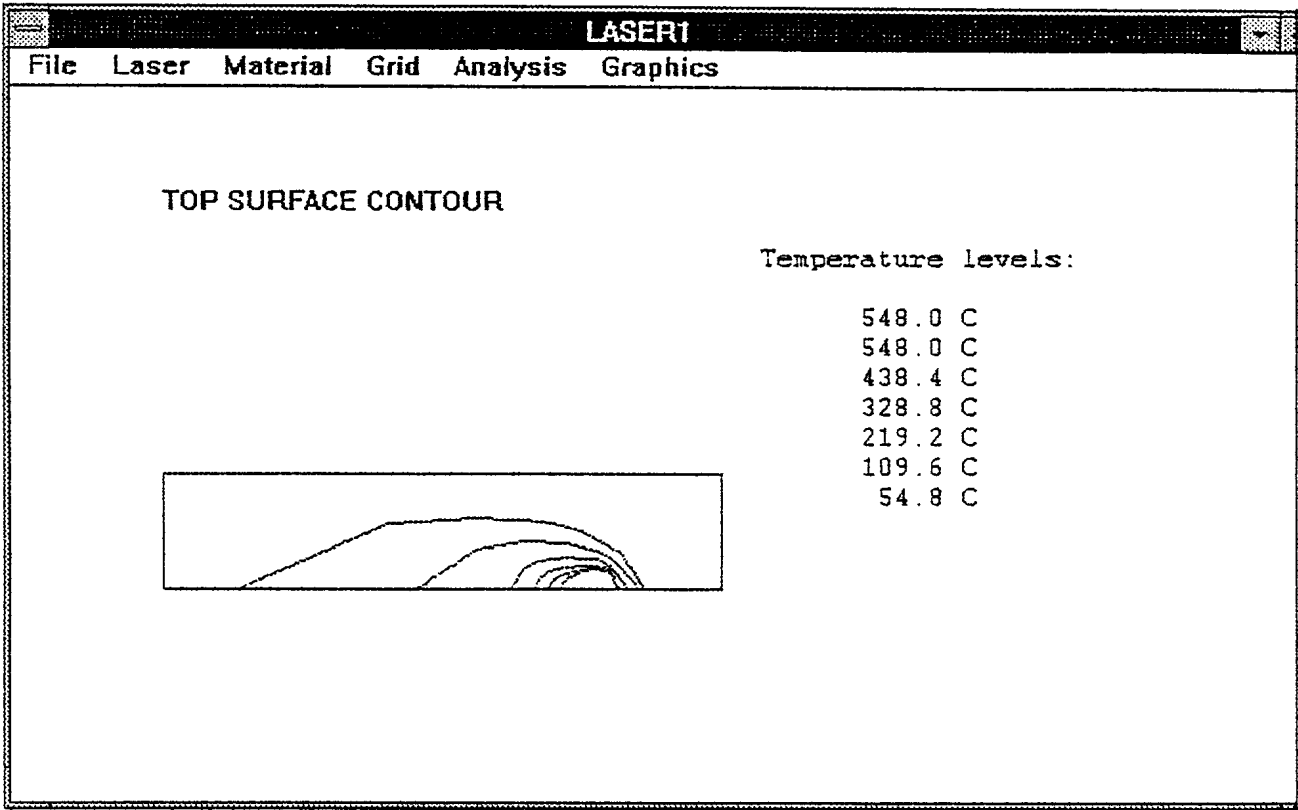


FIGURE B.15: Temperature Contours on the Top Surface

B.20

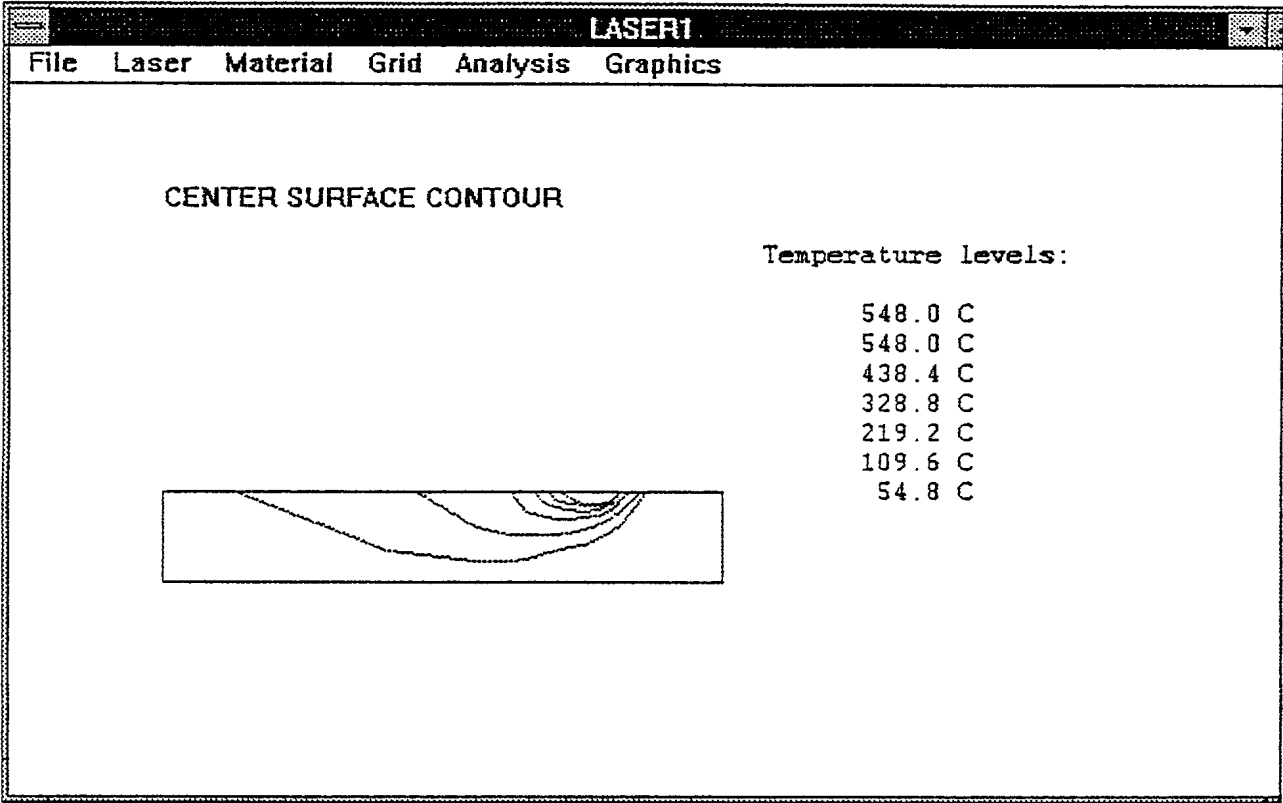


FIGURE B.16: Temperature Contours on the Centre Plane

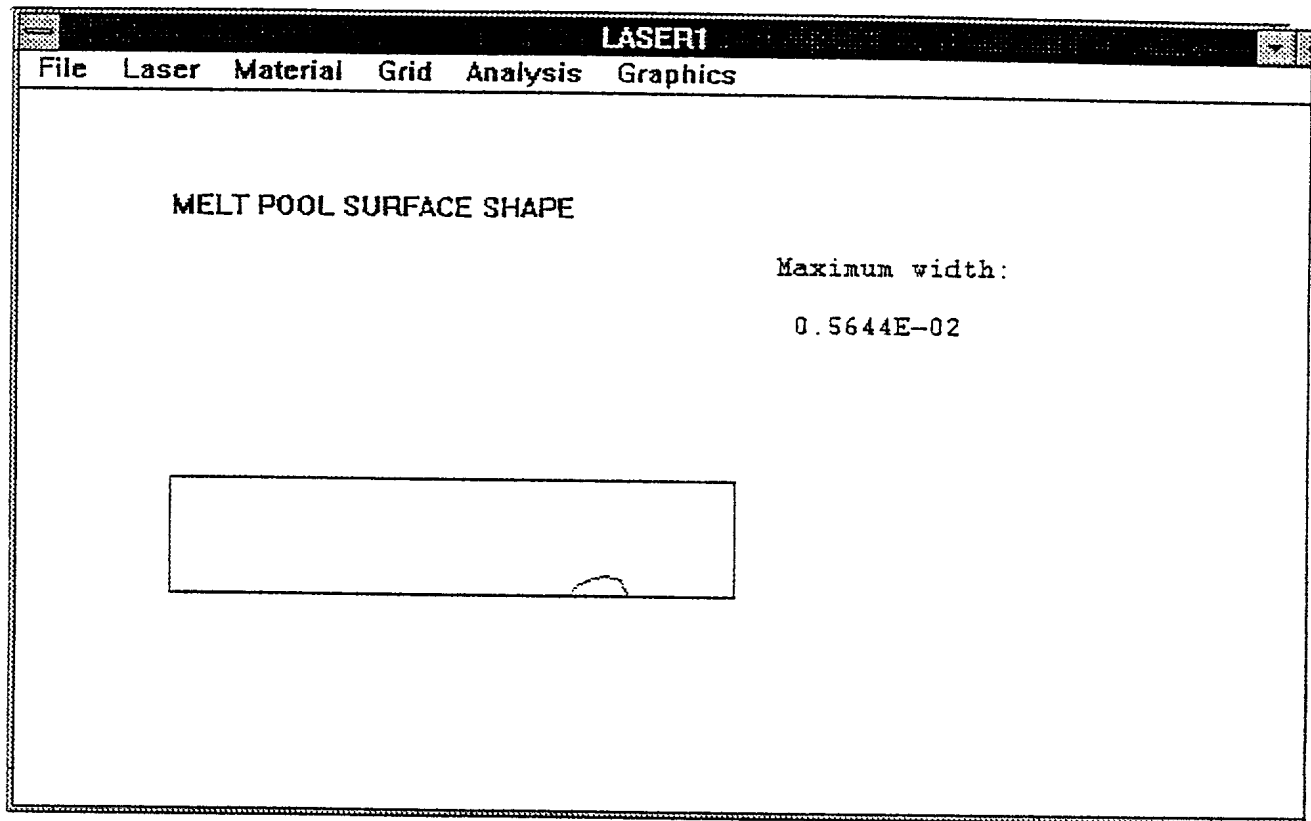


FIGURE B.17: Plan View of the Melt-Pool

B.22

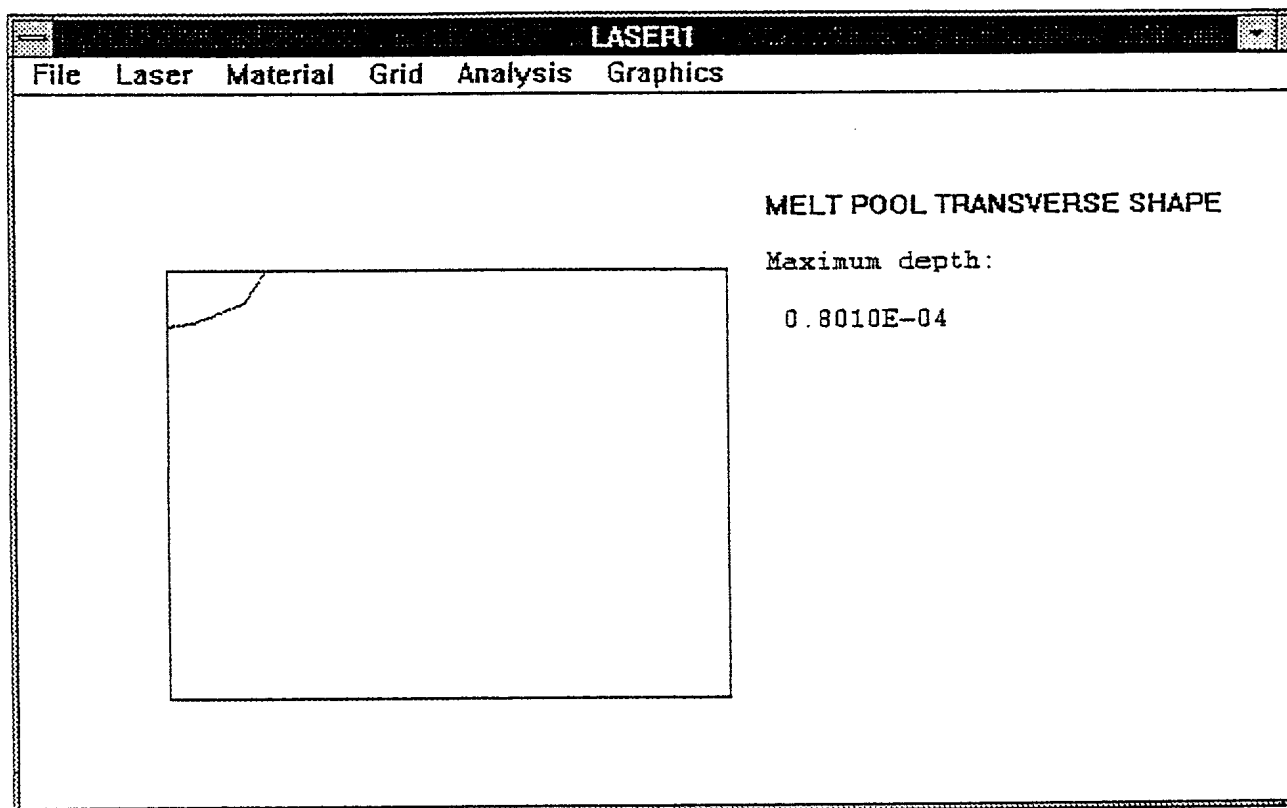


FIGURE B.18: Transverse View of the Melt-Pool

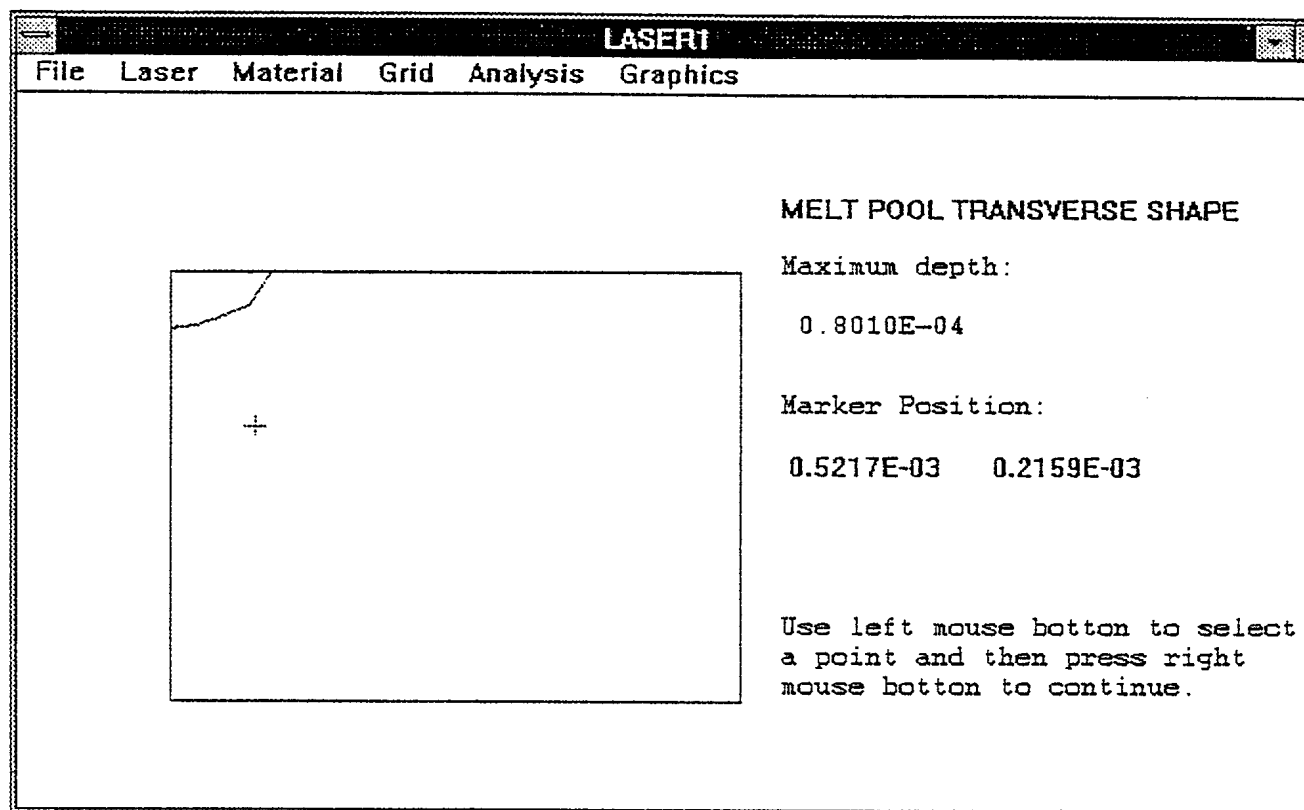


FIGURE B.19a: A Point Selected on the Transverse Section Through the Weld-Pool

B.24

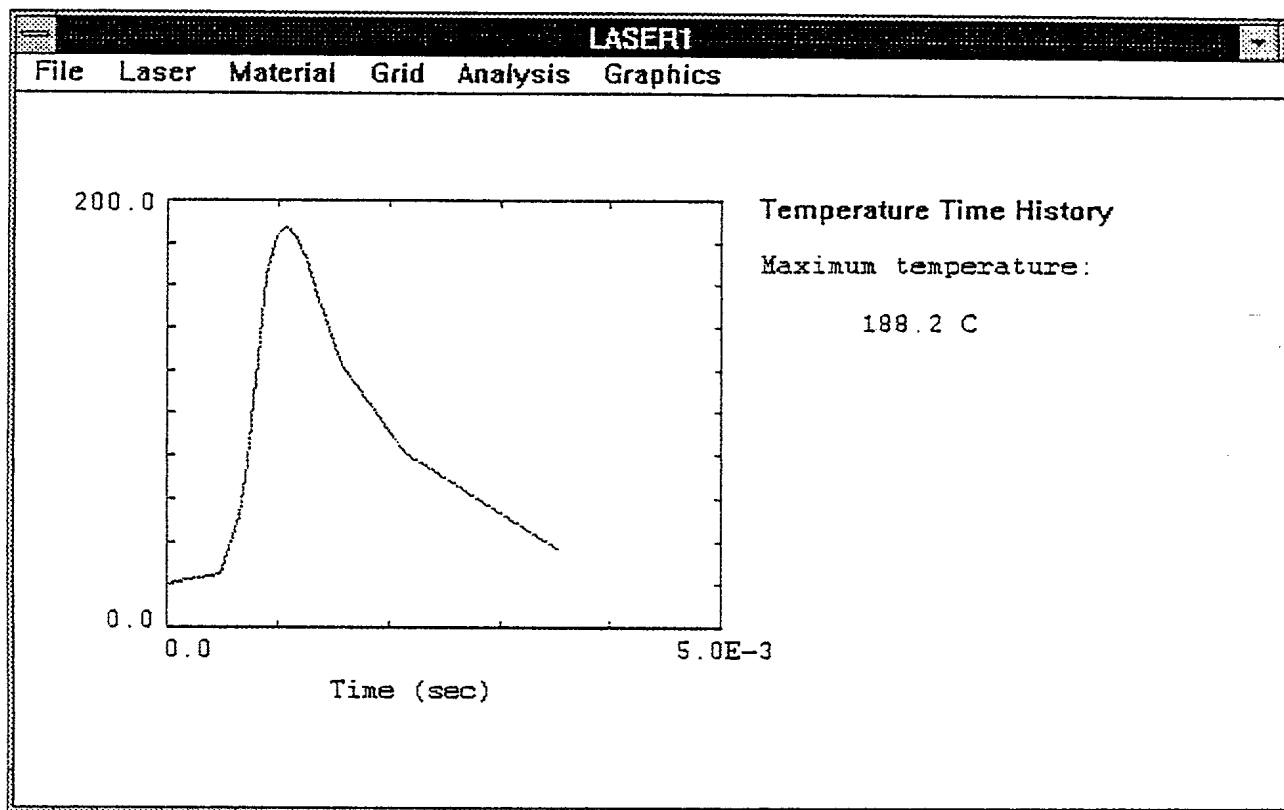


FIGURE B.19b: Temperature Time History for User Selected Point

UNCLASSIFIED
SECURITY CLASSIFICATION OF FORM
(highest classification of Title, Abstract, Keywords)

DOCUMENT CONTROL DATA		
(Security classification of title, body of abstract and indexing annotation must be entered when the overall document is classified)		
1. ORIGINATOR (the name and address of the organization preparing the document. Organizations for whom the document was prepared, e.g. Establishment sponsoring a contractor's report, or tasking agency, are entered in section 8.) Martec Limited 1888 Brunswick Street Halifax, N.S., B3J 3J8	2. SECURITY CLASSIFICATION (overall security classification of the document including special warning terms if applicable). <p style="text-align: center; font-size: large;">Unclassified</p>	
3. TITLE (the complete document title as indicated on the title page. Its classification should be indicated by the appropriate abbreviation (S,C,R or U) in parentheses after the title). <p style="text-align: center; font-size: large;">Computer Modelling of Heat Flow Following Laser Surface Melting</p>		
4. AUTHORS (Last name, first name, middle initial. If military, show rank, e.g. Doe, Maj. John E.) <p style="text-align: center;">Liu, S.B., Liu, Q., Mackay, K.D., Chernuka, M.W.</p>		
5. DATE OF PUBLICATION (month and year of publication of document) <p style="text-align: center;">August 1995</p>	6a. NO OF PAGES (total containing information include Annexes, Appendices, etc). <p style="text-align: center;">47</p>	6b. NO. OF REFS (total cited in document) <p style="text-align: center;">27</p>
7. DESCRIPTIVE NOTES (the category of the document, e.g. technical report, technical note or memorandum. If appropriate, enter the type of report, e.g. interim, progress, summary, annual or final. Give the inclusive dates when a specific reporting period is covered). <p style="text-align: center;">Contractor Report</p>		
8. SPONSORING ACTIVITY (the name of the department project office or laboratory sponsoring the research and development. Include the address). Defence Research Establishment Atlantic P.O. Box 1012 Dartmouth, N.S. B2Y 3Z7		
9a. PROJECT OR GRANT NO. (if appropriate, the applicable research and development project or grant number under which the document was written. Please specify whether project or grant). W7707-4-3145/01-HAL	9b. CONTRACT NO. (if appropriate, the applicable number under which the document was written). <p style="text-align: center;">DREA CR 95/436</p>	
10a. ORIGINATOR'S DOCUMENT NUMBER (the official document number by which the document is identified by the originating activity. This number must be unique to this document). <p style="text-align: center;">TR-95-10</p>	10b. OTHER DOCUMENT NOS. (Any other numbers which may be assigned this document either by the originator or by the sponsor).	
11. DOCUMENT AVAILABILITY (any limitations on further dissemination of the document, other than those imposed by security classification) <div style="font-family: monospace; font-size: small;"> (X) Unlimited distribution () Distribution limited to defence departments and defence contractors; further distribution only as approved () Distribution limited to defence departments and Canadian defence contractors; further distribution only as approved () Distribution limited to government departments and agencies; further distribution only as approved () Distribution limited to defence departments; further distribution only as approved () Other (please specify): </div>		
12. DOCUMENT ANNOUNCEMENT (any limitation to the bibliographic announcement of this document. This will normally correspond to the Document Availability (11). However, where further distribution (beyond the audience specified in 11) is possible, a wider announcement audience may be selected). <p style="text-align: center;">Unlimited</p>		

UNCLASSIFIED
SECURITY CLASSIFICATION OF FORM

DCD03 2/06/87-M

UNCLASSIFIED
SECURITY CLASSIFICATION OF FORM

13. **ABSTRACT** (a brief and factual summary of the document. It may also appear elsewhere in the body of the document itself. It is highly desirable that the abstract of classified documents be unclassified. Each paragraph of the abstract shall begin with an indication of the security classification of the information in the paragraph (unless the document itself is unclassified) represented as (S), (C), (R), or (U). It is not necessary to include here abstracts in both official languages unless the text is bilingual).

A transient three-dimensional heat transfer program called LASER1 which describes the thermal history of a specimen after laser treatment with a scanned continuous laser, has been developed following the experimentally verified method of A.F.A. Hoadley, M. Rappaz and M. Zimmerman [3]. The program was based on the conservation of energy for the treated specimen, and the three-dimensional implicit finite difference method. The surface of the melting pool was assumed to be flat. The fluid dynamics effects of the melting pool were neglected. The properties of the treated material were assumed to be linear functions of temperature for solid phase, but independent of temperature for the liquid phase. A windows-based and easy-to-user interface program, was also developed to guide the users with the provision of the temperature dependent thermal and optical properties of the material, with the provision of the laser beam and operational parameters and with the display of the computational results. The program developed in this report was used to simulate the laser surface melting for the eutectic alloy Al-Cu 33 Wt Pct over a range of traversing speeds between 0.2 to 5.0 m/s. Excellent agreement has been obtained from the comparison between the current simulation results, and the simulation and the experimental results obtained in Reference [3]

14. **KEYWORDS, DESCRIPTORS or IDENTIFIERS** (technically meaningful terms or short phrases that characterize a document and could be helpful in cataloguing the document. They should be selected so that no security classification is required. Identifiers, such as equipment model designation, trade name, military project code name, geographic location may also be included. If possible keywords should be selected from a published thesaurus. e.g. Thesaurus of Engineering and Scientific Terms (TEST) and that thesaurus-identified. If it not possible to select indexing terms which are Unclassified, the classification of each should be indicated as with the title).

Laser
Surface Melting
Heat Flow
Numerical Analysis
Finite Difference Method

155076

UNCLASSIFIED
SECURITY CLASSIFICATION OF FORM